ACS Catalysis

Research Article

pubs.acs.org/acscatalysis

Evidence for the Bifunctional Nature of Pt−Re Catalysts for Selective Glycerol Hydrogenolysis

Derek D. Falcone,[†] John H. Hack,[†] Alexander Yu. Klyushin,[‡] Axel Knop-Gericke,[‡] Robert Schlögl,[‡] and Robert J. Davis*[,†]

[†]Department of Chemical Engineering, University of Virginia, 102 Engineers' Way, PO Box 400741, Charlottesville, Virginia 22904-4741, United States

[‡]Department of Inorganic Chemistry, Fritz-Haber Institut der Max-Planck Gesellschaft, 4-6 Faradayweg, 14195, Berlin, Germany

Supporting Information

ABSTRACT: Rhenium substantially promotes the rate of Pt-catalyzed glycerol hydrogenolysis to propanediols and shifts the product selectivity from 1,2-propanediol to a mixture of 1,2 and 1,3-propanediols. This work presents experimental evidence for a tandem dehydration−hydrogenation mechanism that occurs over a bifunctional Pt−Re catalyst. Infrared spectroscopy of adsorbed pyridine and the rate of aqueous-phase hydrolysis of propyl acetate were used to identify and quantify Brønsted acid sites associated with the Re component. Near-ambient-pressure XPS revealed a range of Re oxidation states on the Pt−Re catalysts after reduction in H_2 at 393 and 493 K, which accounts for the presence of Brønsted acidity. A mechanism involving acid-catalyzed dehydration followed by Pt-catalyzed hydrogenation was consistent with the negative influence of added base, a primary kinetic isotope effect with deuterated glycerol, an inverse isotope effect with dideuterium gas, and the observed orders of reaction.

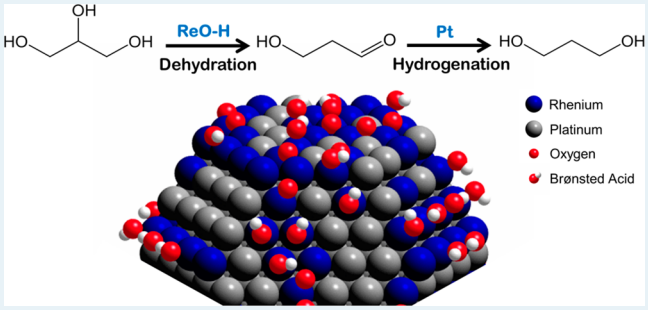

KEYWORDS: *heterogeneous catalysis, bimetallic, biomass, platinum, rhenium, Brønsted acidity, X-ray photoelectron spectroscopy*

1. INTRODUCTION

Interest in bimetallic catalysts consisting of a late transition metal such as Pt together with an oxophilic metal such as Re has increased in recent years because of their potential application in several reactions relevant to the transformation of biomass-derived molecules to fuels and chemicals.[1−14] Although alumina-supported sulfided Pt−Re bimetallic catalysts have been used industrially for decades in naphtha reforming,[15−21] the unsulfided version of this catalyst exhibits a very interesting catalytic performance in liquid water.

In the early 2000s, Dumesic and co-workers reported that platinum group metals catalyze the aqueous phase reforming (APR) of biomass-derived molecules.[22] Soon thereafter, several monometallic and bimetallic catalysts based on transition group metals were developed to reform glycerol, a waste product of triglyceride transesterification to produce biodiesel.[23−25] Promotion of carbon-supported Pt nanoparticles with a second oxophilic metal increased the rate of glycerol reforming to H_2, CO, CO_2, and light alkanes in liquid water by an order of magnitude compared with monometallic Pt.[1−3]

Supported platinum group nanoparticles are also effective catalysts for the hydrogenolysis of glycerol. The hydrogenolysis of glycerol is often carried out at temperatures lower than that for APR to maximize the selectivity to propanediols.[26−29] Daniel et al. reported that the addition of Re to Pt increased the rate of glycerol hydrogenolysis substantially and shifted the product selectivity from almost exclusively terminal hydrogenolysis, which produces 1,2-propanediol (1,2-PDO), toward internal hydrogenolysis, which formed 1,3-propanediol (1,3-PDO).[4] At temperatures as low as 393 K, monometallic Pt, Rh, or Ir catalysts are nearly inactive for glycerol hydrogenolysis, but the addition of Re increases the rate of the reaction in liquid water and increases the selectivity of internal C−O bond hydrogenolysis.[7,30,31] These types of bimetallic catalysts also demonstrate high activity and selectivity for the hydrogenolysis of other α,β-oxygen-substituted substrates, such as 2-(hydroxymethyl)tetrahydropyran and tetrahydrofurfuryl alcohol.[7,32,33] Although a significant amount of work has documented the performance of bimetallic catalysts consisting of Re together with a platinum group metal, the mechanism of hydrogenolysis in liquid water and the promotional role of Re are still unclear.[5−8]

The Tomishige group has studied the hydrogenolysis of different molecules and proposes the role of Re is to act as a Lewis acid. For glycerol hydrogenolysis, they speculate glycerol anchors to the surface through the terminal alcohol group,

Received: July 1, 2015
Revised: August 13, 2015
Published: August 18, 2015

DOI: 10.1021/acscatal.5b01371
ACS Catal. 2015, 5, 5679−5695

Table 1. Results from H_2 Chemisorption and Electron Microscopy of Pt and Pt−Re Catalysts

catalyst	support	Pt[a] (wt %)	Re[a] (wt %)	Re/Pt[b]	H uptake[c] (μmol/g)	H/Pt[c]	av metal diameter[d] (nm)	surface av metal diameter[e] (nm)
8 wt % Pt−Re/SiO_2	silica	8.0	7.6	1.0	155	0.38	2.4 ± 0.95	3.2
8 wt % Pt−Re/SiO_2−W	silica	8.0	7.6	0.89	135	0.33	2.6 ± 0.89	3.2
8 wt % Pt/SiO_2	silica	8.0			118	0.30	4 ± 2.4	8.0
8 wt % Pt−Re/C	carbon	8.0	7.6	0.95	136	0.33	4 ± 3.2	9.6
8 wt % Pt/C	carbon	8.0			16	0.039	7 ± 7.3	27
4 wt % Pt−Re/C	carbon	4.0	3.8	1.0	85	0.41	1.7 ± 0.41	1.9
4 wt % Pt/C	carbon	4.0			56	0.27	2 ± 1.5	5.1

[a]Nominal weight loadings. [b]Molar ratio measured via ICP−OES. [c]Obtained via H_2 chemisorption at 308 K after the catalysts were reduced in situ at 473 K. [d]Obtained via TEM. [e]Obtained via TEM by $\sum d^3/\sum d^2$.

followed by the activation of the internal C−O bond of glycerol by a hydride produced from the heterolytic cleavage of H_2.[5,6]

A different mechanism for hydrogenolysis of oxygenates was proposed by Chia et al.[7] In that work, researchers used results from reaction studies, NH_3 temperature-programed desorption, and density functional theory (DFT) calculations to suggest that a Brønsted acid site is associated with the Re component of the bimetallic catalyst in liquid water. Supported by results from quantum chemical calculations, Chia et al. suggested that protolytic activation preferentially occurred at the internal carbon of glycerol instead of the terminal carbon because secondary carbenium ions are more stable than primary carbenium ions.[7] Following the acid-catalyzed dehydration of glycerol on the speculated acid site associated with Re, the unsaturated reaction intermediate could then be hydrogenated by the late transition metal component of the catalysts (Rh) to form the final product (1,3-PDO). Consistent with the mechanism involving a Brønsted acid site, the ion formation energies of several other oxocarbenium ions showed a strong correlation with the rate of hydrogenolysis of the corresponding oxygenate.[7]

Other works have also suggested that Brønsted acid sites associated with Re are responsible for the increased rate of glycerol APR when Re is added to Pt based catalysts.[12,13,34,35] In addition, FTIR spectroscopy of adsorbed pyridine showed that Brønsted acid sites were present on Pt−Re bimetallic catalysts supported on silica.[12,34] It is unclear from these studies, however, whether Brønsted acid sites are ascribed to the Pt−Re bimetallic nanoparticles or to weakly held perrhenate species on the silica surface.[36] Ciftci et al. also used evidence from CO stripping voltammetry to show that Re is a strong binder of oxygen species, which could facilitate water activation to produce OH species on the surface.[12]

In this work, the bifunctional nature of supported Pt−Re bimetallic catalysts is investigated. The Pt−Re system was chosen because theoretical calculations suggest that Pt−Re bimetallic nanoparticles form the strongest Brønsted acid sites (on the basis of deprotonation energy) compared with other common bimetallic systems containing a reducible metal and an oxophilic metal.[7,37] Glycerol hydrogenolysis in the presence of NaOH, diffuse reflectance infrared Fourier transform spectroscopy (DRIFTS) of adsorbed pyridine, and propyl acetate hydrolysis were used to gain critical insights into the role of the Re component in bimetallic Pt−Re nanoparticles for glycerol hydrogenolysis. In addition, the kinetics of glycerol hydrogenolysis were investigated by varying glycerol concentration and H_2 pressure as well as measuring the kinetic isotope effect using glycerol$(OH)_3$-d_5 and D_2.

The oxidation state of Re in the working state of the bimetallic catalysts is still unknown, even though the oxidation state of Re in Pt−Re bimetallic catalysts has been under investigation for several decades.[38] One of the reasons for the ambiguity regarding the oxidation state of Re is its dependence on the conditions to which the Re is subjected. The reduction of Re^{7+}, or perrhenate (the most stable oxidation state), usually does not begin until ∼573 K,[39] but it can occur as low as 373 K in the presence of Pt because of hydrogen spillover.[4] Because Re is oxophilic, the partially reduced Re in the Pt−Re bimetallic catalyst is oxidized to Re^{7+} upon exposure to air. Therefore, the oxidation state of Re depends on the pretreatment of the catalyst and the conditions under which the catalyst is probed.[35]

Recently, in situ X-ray absorption spectroscopy (XAS) has been used to study Pt−Re particles supported on Norit carbon[4] as well as Rh−Re[40] and Ir−Re[41] particles supported on silica. The average oxidation state of Re in those works was determined to be ∼2+ after reduction in flowing H_2 at temperatures between 373 and 473 K. Another study by Chia et al. concluded that Re in Rh−Re nanoparticles supported on Vulcan carbon were metallic.[8] Interestingly, that work showed that the oxidation state of Re was the same in gaseous H_2 as under reaction conditions with H_2-saturated water.

In the current study, X-ray photoelectron spectroscopy was used to study the oxidation state of Re in Pt−Re bimetallic catalysts supported on both Vulcan carbon and silica. The advantages of using XPS are that the various oxidation states can be discerned instead of an overall bulk average, and the technique is more sensitive to the elemental composition at the surface, which is most applicable to catalysis. In addition to using conventional XPS equipped with an Al $K\alpha$ radiation source, experiments were performed using a near-ambient pressure X-ray photoelectron spectrometer (NAP-XPS), which allowed for measurements to take place in the presence of H_2 and water vapor at 393 and 473 K.

2. RESULTS

2.1. Catalyst Characterization. The properties of the supported bimetallic catalysts used in this study are summarized in Table 1. Silica gel and Vulcan carbon were used as supports to permit interrogation of the Pt−Re nanoparticles by infrared spectroscopy and NAP-XPS, respectively. All of the catalyst studied in this work had a 1:1 nominal molar ratio of Pt to Re, and the naming convention used describes only the weight loading of Pt. For example, as shown in Table 1 the catalyst named 8 wt % Pt−Re/SiO_2 had a Pt weight loading of 8% and a Re weight loading of 7.6%, which corresponds to a 1:1 molar ratio of Pt and Re.

DOI: 10.1021/acscatal.5b01371
ACS Catal. 2015, 5, 5679−5695

Table 2. Results from Glycerol Hydrogenolysis over 8 wt % Pt−Re/SiO_2, 8 wt % Pt−Re/SiO_2−W, and 8 wt % Pt−Re/C[a]

					selectivites (%)				
catalyst	time (min)	conversion (%)	rate (μmol $g^{-1}min^{-1}$)	TOF[b] (s^{-1})	1,2-PDO	1,3-PDO	2-Prop	1-Prop	sec/prim
8 wt % Pt−Re/SiO_2	60	8.3	98	0.0105	40	24	11	25	0.55
8 wt % Pt−Re/SiO_2−W	90	9.1	59	0.0073	36	29	11	23	0.64
8 wt % Pt−Re/C	240	6.5	17	0.0021	33	34	9	27	0.77

[a]Reaction conditions: 393 K, 4 MPa H_2, 90 cm^3 110 mM glycerol solution, Gly/Re = 150. In situ pretreatment: 393 K, 1.4 MPa H_2 for 1 h. [b]Normalized by H chemisorption uptake.

Dihydrogen chemisorption was used to estimate the number of exposed Pt sites on the bimetallic catalysts. Previous studies revealed that the uptake of chemisorbed hydrogen on supported monometallic Re catalysts is below the detection limit.[4] The results in Table 1 show the bimetallic catalysts chemisorbed more hydrogen compared with the monometallic Pt catalysts, indicating a greater fraction of the Pt was exposed. This is partly attributed to the fact that the Pt−Re catalysts had smaller particle sizes compared with the monometallic Pt catalysts, as revealed by TEM. This trend was especially evident on the carbon-supported catalysts. The bimetallic 8 wt % Pt−Re/C catalyst had a significantly higher H/Pt ratio than the 8 wt % Pt/C catalyst, and the number-average particle size measured by TEM was about half the size of the monometallic catalyst. Moreover, the monometallic Pt/C catalyst also had a much broader particle size distribution that included some particles >20 nm. In fact, the bimetallic catalysts had narrower particle size distributions compared with the corresponding monometallic catalysts, regardless of support. The particle size distributions for the catalysts in Table 1 are depicted in Figure S1. The consistently smaller particle sizes of the Pt−Re bimetallic catalysts indicates a stabilization of Pt against sintering at elevated temperatures by the presence of Re.[2,42]

Table 1 also summarizes the properties of 8 wt % Pt−Re/SiO_2−W, which is a catalyst that has been "washed" to remove weakly held, water-soluble perrhenate that was not associated with the Pt on 8 wt % Pt−Re/SiO_2. Vicente et al. report that Re catalysts synthesized via incipient wetness impregnation of aqueous perrhenate results in well-dispersed but weakly held species on silica supports.[36] Therefore, it is likely that some weakly held perrhenate ions were present on the silica-based Pt−Re bimetallic catalysts used in this work and others reported previously. In addition, silica-supported perrhenate has been shown to expose Brønsted acid sites.[12] The washing procedure is described in Section 5.1.

2.2. Polyol Hydrogenolysis. *2.2.1. Glycerol Hydrogenolysis.* The rates and selectivities of glycerol hydrogenolysis at 393 K in a 110 mM aqueous glycerol solution with 4 MPa of H_2 over 8 wt % Pt−Re/SiO_2, 8 wt % Pt−Re/SiO_2−W, and 8 wt % Pt−Re/C are presented in Table 2. Two measures of activity are presented: one normalized to the mass of the catalyst, and the other normalized to the hydrogen uptake measured via H_2 chemisorption to give a turnover frequency (TOF). The TOF is one way to report a rate that properly accounts for differences in exposed metal attributed to differences in particle size. Unfortunately, the different affinities of Re and Pt for hydrogen means that the TOF expressed here is still based on an approximation of exposed active sites. Nevertheless, we observed that the Pt−Re nanoparticles supported on silica had a higher activity per mass of catalyst as well as a higher TOF compared with the carbon-supported bimetallic catalyst. Although the rate was higher on the silica-supported catalyst, the Sec/Prim ratio (a ratio of internal hydrogenolysis products to terminal hydrogenolysis products defined in Section 5.1) was lower on the silica-supported catalyst when compared with carbon-supported catalyst, indicating that the carbon-supported catalyst was more selective to internal hydrogenolysis reactions. In general, at 393 K in a 110 mM aqueous glycerol solution with 4 MPa of H_2, we observed the Sec/Prim ratio on silica-supported bimetallic catalysts to range between 0.5 and 0.6, whereas the ratio on the carbon-supported bimetallic catalysts was between 0.65 and 0.8. The Sec/Prim ratio was relatively independent of the glycerol conversion, up to 55%. Even though the addition of Re shifts the product selectivity to 1,3-PDO, corresponding to an increase in the Sec/Prim ratio, 100% selectivity to products resulting from the activation of secondary C−O bonds was never obtained, and primary C−O bond activation over Pt−Re was always observed. As explained by Chia et al., a possible intermediate for the hydrogenolysis of glycerol was found to be an oxirane-type carbocation formed via dehydration and ring closure. Ring opening of the oxirane carbocation can lead to either terminal alcohol (1,3-PDO) or secondary alcohol (1,2-PDO), depending on which bond is activated.[7] We suspect this is why very high selectivity to 1,3-PDO is never achieved with glycerol. A time profile of glycerol hydrogenolysis on 8 wt % Pt−Re/SiO_2 is presented in the Supporting Information (Figure S2).

As seen in Table 2, the rate of glycerol hydrogenolysis per mass of catalyst of the washed catalyst (8 wt % Pt−Re/SiO_2−W) was ∼60% of the rate of the unwashed catalyst (8 wt % Pt−Re/SiO_2), whereas the Sec/Prim ratio was slightly higher on the washed catalyst. To wash the catalyst, liquid water, which was purged with N_2 and saturated with H_2, flowed over the catalyst at a rate of 2 cm^3 min^{-1} for approximately 30 min. In Table 1, ICP-OES results show that the Re/Pt ratio decreased by ∼11%, indicating that some Re was removed from the catalyst as a result of washing. In addition, the hydrogen uptake measured via H_2 chemisorption decreased slightly. The particle size analysis, however, showed that the metal particle size did not change significantly during the washing procedure. In light of the reactivity results in Table 2, we conclude that the washing procedure did not significantly alter the nature of the active sites. As discussed later, the weakly held, soluble perrhenate that is removed during the washing treatment is inactive for glycerol hydrogenolysis. A small decrease in glycerol hydrogenolysis activity following the washing treatment suggests that some active Re associated with the Pt is removed during washing. The main goal of the washing procedure, however, was to ensure that all soluble perrhenate was removed from the catalyst.

The monometallic Pt/SiO_2 catalyst demonstrated a glycerol conversion of only 0.3% after 34 h of reaction at 393 K (utilizing three times the catalyst loadings used for results in Table 2), which corresponds to a TOF over monometallic Pt of 4.2×10^{-6} s^{-1}. Conversion of glycerol was not observed on 8 wt % Pt/C at 393 K because of its very low dispersion of Pt.

DOI: 10.1021/acscatal.5b01371
ACS Catal. 2015, 5, 5679−5695

Daniel et al. showed that at 473 K, a temperature at which monometallic Pt supported on Norit activated carbon had some measurable activity, the TOF of their Pt−Re/C catalyst was over an order of magnitude higher than Pt/C. That study also showed that their carbon-supported monometallic Re catalyst was inactive for glycerol hydrogenolysis at 473 K.[4] Clearly, the promotional effect of adding Re to supported Pt catalysts was observed, regardless of the support.

Switching the Pt precursor used to make 8 wt % Pt−Re/SiO_2 from $Pt(NH_3)_4(NO_3)_2$ to H_2PtCl_6 decreased the TOF of hydrogenolysis by almost 50%, but the Sec/Prim ratio changed only from 0.47 to 0.39 at 7% conversion. Interestingly, the change in Pt precursor only slightly decreased the rate of hydrogenolysis and the Sec/Prim ratio when Vulcan carbon was used as the support, as shown in the Supporting Information (Table S1).

Li and coauthors have studied glycerol hydrogenolysis extensively using bifunctional catalysts consisting of Pt and different heteropolyacids (HPA) supported on zirconia.[43−46] They observed a very strong correlation between the number of Brønsted acid sites, measured by the FTIR spectroscopy of adsorbed pyridine, and the yield of 1,3-PDO from glycerol hydrogenolysis at 453 K. Their work suggests that the Brønsted acid sites on the HPA's contribute to the production of 1,3-PDO, presumably by acid-catalyzed dehydration, followed by Pt-catalyzed hydrogenation.

2.2.2. Glycerol Hydrogenolysis Using Heterogeneous Pt and Homogeneous Acid. An experiment was performed to test whether it was sufficient to have the acid in solution together with supported Pt particles to produce 1,3-PDO during glycerol hydrogenolysis. An amount of HCl that was equivalent to the moles of Re on the 8 wt % Pt−Re/SiO_2 was added to the reaction medium with the monometallic 8 wt % Pt/SiO_2 catalyst. The reaction with HCl and 8 wt % Pt/SiO_2 had a TOF of only 5.5×10^{-5} s^{-1} at very low conversion compared with a TOF of 0.0105 s^{-1} observed on the bimetallic catalyst. Because the TOF on 8 wt % Pt/SiO_2 in the absence of HCl was 4.2×10^{-6} s^{-1}, the addition of HCl increased the rate by an order of magnitude, but it was still several orders of magnitude slower than 8 wt % Pt−Re/SiO_2.

Another control reaction was conducted in which soluble $HReO_4$ was added to the reaction medium, together with 8 wt % Pt/SiO_2. In this experiment, the molar ratio of Re and Pt was also chosen to be 1:1. The TOF (based on exposed Pt) for the reaction with the $HReO_4$ and 8 wt % Pt/SiO_2 was 1.6×10^{-4} s^{-1}, which was nearly 300% higher than the TOF for 8 wt % Pt/SiO_2 with HCl. The increase in rate with the addition of Re suggests that perrhenate in solution may reduce onto the Pt nanoparticles during the course of the reaction and form the active sites that are present on the Pt−Re bimetallic catalyst. It also must be noted that the experiments with HCl and $HReO_4$ added to the reaction with 8 wt % Pt/SiO_2 demonstrated Sec/Prim ratios of 1.0 and 0.9, respectively, indicating internal C−O bond activation is more favored in acidic solutions. Moreover, both Pt and acid are required for high activity because conversion of glycerol was not observed in the presence of only acid. The results from experiments with the homogeneous acids and supported Pt, considered together with the work conducted by Li and coauthors,[43−46] suggest that intimate contact of the Brønsted acid site and a Pt metal site is required to produce 1,3-PDO at a high rate from glycerol.

2.2.3. Kinetics of Glycerol Hydrogenolysis on 8 wt % Pt−Re/SiO_2. Figure 1 shows the rate of glycerol hydrogenolysis

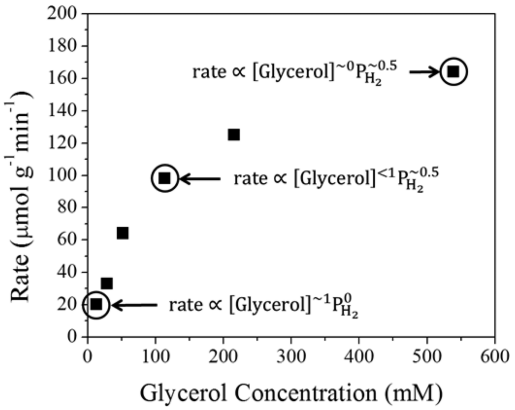

Figure 1. Initial rate of glycerol hydrogenolysis at 393 K and 4 MPa of H_2 in different initial concentrations of glycerol.

measured over a wide range of glycerol concentrations (15 to 550 mM) after 1 h of reaction. The conversions and selectivities for these experiments are presented in the Supporting Information (Table S2). As illustrated in Figure 1, the reaction order in glycerol approached zero at high concentrations, suggesting that the catalytic surface was nearly saturated with a glycerol-derived species at concentrations above 550 mM. In contrast, the rate of hydrogenolysis was approximately first-order in glycerol at low concentrations. Chia et al. studied tetrahydrofurfuryl alcohol hydrogenolysis on a carbon-supported Rh−Re catalyst and also reported a first-order dependence on tetrahydrofurfuryl alcohol concentration in the range of 94 to 439 mM.[7] Tomishige and coauthors, however, observed the rate of tetrahydrofurfuryl alcohol hydrogenolysis on both silica-supported Rh−Re and Ir−Re catalysts,[47] and the rate of glycerol hydrogenolysis on silica-supported Rh−Re[48] and Ir−Re[6] catalysts to be zero-order in reactant. Those studies of cyclic ether and polyol hydrogenolysis in liquid water by Tomishige et al. involved substrate concentrations of ∼2 M or higher. Thus, the kinetics were most likely measured in the surface saturation regime for both tetrahydrofurfuryl alcohol and glycerol.

In the current work, an interesting trend between the Sec/Prim and the concentration of glycerol was observed (Table S2). As the concentration of glycerol increased from 15 to 550 mM, the Sec/Prim ratio increased from 0.55 to 0.67, indicating that the catalyst was more selective to internal hydrogenolysis reactions at higher concentrations of glycerol.

The order of reaction in H_2 was also investigated for glycerol hydrogenolysis. The H_2 order was measured at three different glycerol concentrations (15, 110, and 550 mM) on 8 wt % Pt−Re/SiO_2. Those results are tabulated in Table S3 and summarized in Figure 1. At the lowest concentration of glycerol studied (15 mM), the order of H_2 was essentially zero because the rate of glycerol hydrogenolysis was ∼20 μmol $g^{-1}min^{-1}$ when the H_2 pressure was varied from 2 to 8 MPa. The observed zero-order behavior suggests that saturation coverage of hydrogen is achieved on the Pt−Re catalyst under very low glycerol concentrations. The order of reaction in H_2 at higher concentrations of glycerol (110 and 550 mM), however, was quite close to 0.5, which is a result typical of equilibrated dissociative adsorption of H_2 during hydrogenation reactions. Interestingly, the study by Chia et al.[7] and the works by Tomishige and coauthors[47,48] reported first-order kinetics in H_2 pressure for cyclic ether and glycerol hydrogenolysis on carbon-

DOI: 10.1021/acscatal.5b01371
ACS Catal. 2015, 5, 5679−5695

Table 3. Effect of Solvent on Hydrogenolysis of 1,2-Hexanediol over 8 wt % Pt−Re/SiO_2[a]

solvent	time (min)	conversion (%)	rate (μmol $g^{-1}min^{-1}$)	TOF[b] (s^{-1})	rate of production (μmol $g^{-1}min^{-1}$) 1-hexanol	2-hexanol	Sec/Prim
water	120	9.5	48	0.0052	41	7	5.50
n-heptane	240	9.1	23	0.0025	14	8	1.60

[a]Reaction conditions: 8 wt % Pt−Re/SiO_2, 393 K, 4 MPa H_2, 110 mM 1,2-HDO solution, Gly/Re = 150. In situ pretreatment: 393 K, 1.4 MPa H_2 for 1 h. [b]Normalized by H_2 chemisorption uptake.

supported Rh−Re catalysts and silica-supported Rh−Re and Ir−Re catalysts, respectively. First-order behavior in H_2 was not observed during glycerol hydrogenolysis over 8 wt % Pt−Re/SiO_2 under conditions investigated in this work.

A reaction was also performed with N_2 in the head space instead of H_2 with a 110 mM glycerol solution at 393 K. For this experiment, the normal in situ reduction of the catalyst was performed, but prior to adding the reactant solution, the reactor was purged four times with N_2, and then 1 MPa of N_2 was added and maintained throughout the course of the reaction. In the absence of added H_2, the typical glycerol hydrogenolysis products were still observed (1,2-PDO, 1,3-PDO, 1-propanol (1-Prop), and 2-propanol (2-Prop)), even after the catalytic site turned over several hundred times. The reaction with N_2 in the head space, however, also yielded several additional products that were not observed in the presence of H_2, which include acetone, propanal, acetic acid, propanoic acid, and ethanol (observed by GC/MS). The appearance of oxygenates containing carbonyls may be the result of glycerol dehydration. The Brønsted acid-catalyzed dehydration of an alcohol group in glycerol produces an enol, which is rapidly converted in liquid water to a ketone or an aldehyde via keto−enol tautomerization.[49−51] We suspect that these products are not observed during reactions in high pressure H_2 because of the rapid hydrogenation of these intermediates. Alternatively, glycerol may act both as the substrate and as the source of hydrogen. Other works observed that secondary alcohols can act as the hydrogen source to reduce polyols instead of H_2 following a Meerwein−Ponndorf−Verley reaction mechanism.[52−54] Small amounts of hydrogen may also be formed by APR of glycerol over metal catalysts in liquid water.[3,13,54] For example, King et al. observed the evolution of 1,2-PDO, 1-Prop, and 2-Prop in the liquid phase during the APR of glycerol over supported Pt−Re particles at 498 K.[3]

The mechanism of glycerol hydrogenolysis was further investigated by probing a kinetic isotope effect with deuterated glycerol, which will be referred to as glycerol$(OH)_3$-d_5. In particular, we measured the rate of hydrogenolysis of glycerol in which all C−H groups were replaced with C−D groups. Using a 15 mM glycerol solution with 4 MPa of H_2, a primary kinetic isotope effect of 2.0 ± 0.1 was observed at 393 K. A kinetic isotope effect ($rate_H/rate_D$) of ∼2 was also measured in experiments with 4 MPa of H_2 in which the glycerol concentration was 110 and 550 mM. As a control experiment, hydrogenolysis of glycerol (both labeled and unlabeled) was also tested using D_2O as the solvent. No influence of using D_2O instead of H_2O as the solvent was observed. The kinetic isotope effect of D_2 was also measured using a 15 mM aqueous solution of normal glycerol and 1 MPa of H_2 (D_2) at 393 K. Interestingly, a kinetic isotope effect ($rate_H/rate_D$) of ∼0.7 was measured when D_2 was used as the reactant gas, indicating that the rate of glycerol hydrogenolysis was faster with D_2.

2.2.4. Polyol Hydrogenolysis on 8 wt % Pt−Re/SiO_2 in an Alkane Solvent. To better understand the role of water in the reaction, hydrogenolysis experiments were also performed using alkane (*n*-heptane) as the solvent. Because the solubility of glycerol in *n*-heptane is extremely low, 1,2-hexanediol (1,2-HDO) was used as the model polyol substrate because its solubility is relatively high in both water and *n*-heptane. The 1,2-HDO hydrogenolysis results over 8 wt % Pt−Re/SiO_2 using water or *n*-heptane as the solvent are presented in Table 3. The observed rate of 1,2-HDO hydrogenolysis was 23 and 48 μmol $g^{-1}min^{-1}$ in *n*-heptane and water, respectively, indicating water is not required to perform hydrogenolysis of 1,2-HDO. The rate of 2-hexanol production, which is produced by activating a primary C−O bond in 1,2-HDO, was the same regardless of the solvent used. The rate of 1-hexanol production, on the other hand, was four times higher when water was used as the solvent compared with heptane. The monometallic 8 wt % Pt/SiO_2 catalyst was inactive for 1,2-HDO hydrogenolysis at 393 K in both water and *n*-heptane, indicating that the Re component of the catalyst is crucial for catalysis and the mechanism of 1,2-HDO hydrogenolysis on Pt−Re bimetallic nanoparticles is similar to that of glycerol hydrogenolysis. The results from hydrogenolysis of 1,2-HDO over 8 wt % Pt−Re/SiO_2 also agree very well with work that was previously performed by Nakagawa et al., who studied the hydrogenolysis of 1,2-HDO in *n*-heptane on Ir−Re/SiO_2.[55]

2.3. X-ray Photoelectron Spectroscopy of Pt−Re Catalysts. *2.3.1. Conventional X-ray Photoelectron Spectroscopy.* X-ray photoelectron spectroscopy was used to ascertain the oxidation states of Pt and Re after the supported nanoparticles were reduced at the moderate temperatures used in the reaction conditions of this study. Before measurements of the catalysts were performed, conventional XPS of Re standards was conducted using Al Kα radiation, the spectra of which are shown in Figure S3. All of the Re standards were characterized "as is" from the manufacturer with no further pretreatment. Multiple Re oxidation states were observed in all of the spectra because the surfaces of the samples readily oxidize in air. In fact, the most thermodynamically stable Re oxide is Re_2O_7.[39] Because Al Kα radiation at 1486.6 eV was used to measure photoemission spectra of the Re standards, the inelastic mean free path of the electrons was ∼1.6 nm, which means photoelectrons from the bulk material will also contribute to the overall signals.[56] The majority of the photoemission response in the conventional XP spectra (Figure S3) of Re metal (Re^0), ReO_2 (Re^{4+}), and ReO_3 (Re^{6+}) standards can be ascribed to the bulk material. The Re $4f_{7/2}$ binding energies for Re^0, Re^{4+}, and Re^{6+} were 40.5, 42.6, and 43.5 eV, respectively, and compare well with reported values.[38,39,57] To estimate the binding energy of Re^{7+}, NH_4ReO_4 was used as the standard because this particular Re salt was used to prepare the catalysts. Two Re species were observed in this sample, which had $4f_{7/2}$ peaks at 45.7 and 47.4

DOI: 10.1021/acscatal.5b01371
ACS Catal. 2015, 5, 5679−5695

eV. The 47.4 eV $4f_{7/2}$ peak has been observed by others for NH_4ReO_4, whereas a 45.7 eV $4f_{7/2}$ peak is most likely attributed to Re_2O_7.[39,58,59] In addition to features associated with the stable bulk oxides of Re, a $4f_{7/2}$ peak with a binding energy of 41.5 eV was also observed in the spectrum of Re metal (Figure S3), which has been ascribed to ReO (Re^{2+}).[39,57] It should be noted that ReO is not stable as a bulk material, but it has been observed at the interface of higher oxidation state oxides and Re metal.[39,57,60]

Once the binding energies for all of the standard Re oxide peaks were determined, the photoemission spectra of Pt−Re catalysts were then analyzed using the CasaXPS fitting software with constraints that are described in Section 5.5. The Pt 4f and Re 4f conventional XP spectra of 8 wt % Pt−Re/C and 8 wt % Pt−Re/SiO_2, exposed to air without in situ reduction, are shown in Figure 2. Even without in situ reduction, the Pt 4f

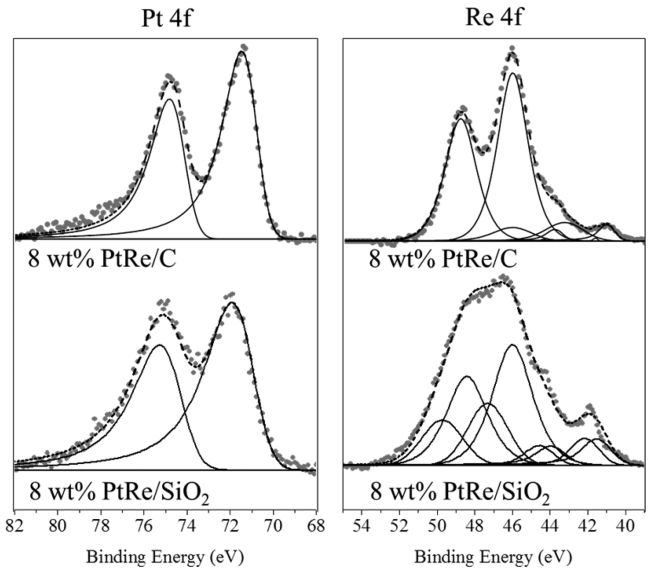

Figure 2. Spectra from conventional XPS of 8 wt % Pt−Re/C and 8 wt % Pt−Re/SiO_2 without in situ reduction. The gray dots are the data, and the dotted black lines are the results from peak fitting.

spectra in Figure 2 reveal binding energies for the $4f_{7/2}$ and $4f_{5/2}$ peaks of ∼71.1 and 74.4 eV, respectively, which correspond to metallic Pt. In fact, the spectra for all of the catalysts studied in this work revealed that Pt was always metallic. The results for the Re binding energies, however, depended strongly on the pretreatment conditions.

Figure 2 also shows the 4f photoemission spectra of the Re component of the catalysts with results from curve-fitting tabulated in Table 4. In contrast to Pt, the Re component of the bimetallic catalysts oxidizes readily when exposed to air.[4] In addition, the degree of Re oxidation by air exposure was different on the two catalysts studied. The peak fitting results show that most of the Re in 8 wt % Pt−Re/C had an oxidation state of Re^{7+}, which is consistent with the previously reported XANES of Pt−Re bimetallic catalysts supported on Norit activated carbon.[4] The conventional XPS results from this work also revealed that a very small portion of the Re was present as Re metal (Re^0) and ReO_2 (Re^{4+}). For the silica-supported catalyst, the Re component of the catalyst was more evenly distributed among the various oxidation states corresponding to Re^0, Re^{2+}, Re^{4+}, and Re^{7+}. In addition, two peaks with binding energies of 47.4 and 49.8 eV were observed, which are close to

Table 4. Composition and Distribution of Re Oxidation States in 8 wt % Pt−Re/C and 8 wt % Pt−Re/SiO_2 Catalysts Evaluated by Conventional XPS[a]

	Distribution of Re Oxidation States				
reduction temperature	Re(0), %	Re(II), %	Re(IV), %	Re(VII), %	Re/Pt
	8 wt % Pt−Re/C				
no reduction	7	0	11	81	1.80
393 K	39	13	45	3	1.78
473 K	59	11	31	0	2.21
	8 wt % Pt−Re/SiO_2				
no reduction	0	13	9	77[b]	3.63
393 K	30	34	36	0	0.67
473 K	51	44	6	0	0.60

[a]Results were determined from curve-fitting of the spectra acquired at room temperature. Some of the catalysts were reduced in situ in H_2 and then evacuated for 5 min prior to analysis. [b]Contains the contribution from the Re $4f_{7/2}$ and $4f_{5/2}$ peaks with binding energies of 47.4 and 49.8 eV, respectively.

the binding energies of peaks observed in the spectra of NH_4ReO_4 (Figure S3). Because the NH_4ReO_4 precursor should have decomposed during the 723 K reduction treatment used in the catalyst synthesis procedure, we ascribe these peaks to Re^{7+}-like species,[38,59] which are well dispersed but weakly held on the silica support.[36] Peaks with binding energies of 47.4 and 49.8 eV were not observed in the 8 wt % Pt−Re/C catalyst, even though the same reduction conditions were used for the 8 wt % Pt−Re/SiO_2 catalyst during synthesis. Evidently, the weakly held perrhenate species was not as stable on the carbon support after the reduction treatment as it was on silica.

The carbon-supported and silica-supported bimetallic catalysts were also studied after reduction in H_2 at 393 and 473 K in a cell attached to the conventional XPS system. Great care was taken to ensure that significant oxidation of the samples did not occur while they were being transferred from the reduction cell to the analysis chamber. To test the level of oxidation that might occur during the transfer, an experiment was performed during which the samples were left in the preparation chamber at 10^{-6} mbar for 90 min after reduction. These samples were compared with those that were transferred as quickly as possible through the preparation chamber, which was ∼5 min. The percent contribution of each Re oxidation state from the curve-fitting results of the Re 4f XP spectra for these experiments is summarized in the Supporting Information (Table S4). Even though the pressure in the preparation chamber was maintained at 10^{-6} mbar, some oxidation of the rhenium was observed after 90 min. This result shows that the rate of Re oxidation is extremely fast, and great care must be taken to keep the Re reduced during reaction and characterization experiments. To determine the significance of the oxidation that occurred after 5 min, the percent contributions of the Re oxidation states at the 5 and 90 min time points were extrapolated to time zero, assuming a linear fit, which are also shown in the Supporting Information (Table S4) in italicized text. This extrapolation suggests that the oxidation occurring after 5 min in the preparation chamber was minimal and that the state of the catalysts after 5 min in the chamber closely resembles the state of the catalyst under reduced conditions.

Conventional XPS results from the curve-fitting of spectra for the catalysts reduced at 393 and 473 K in H_2 are also summarized in Figure 3 and Table 4. As mentioned previously,

DOI: 10.1021/acscatal.5b01371
ACS Catal. 2015, 5, 5679−5695

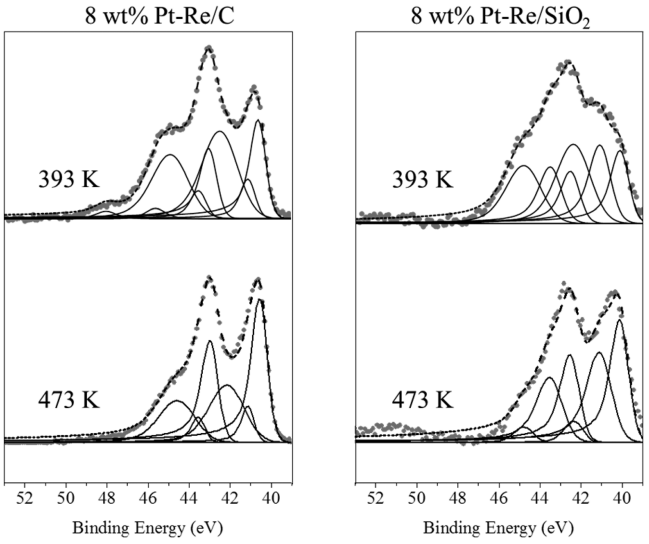

Figure 3. Re 4f spectra from conventional XPS of 8 wt % Pt−Re/C and 8 wt % Pt−Re/SiO_2 reduced at 393 and 473 K after only 5 min in the preparation chamber. The gray dots are the data, and the dotted black lines are the results from peak fitting.

the Pt 4f spectra revealed that Pt was always in the metallic state on the samples, regardless of how the catalysts were pretreated prior to XPS. In contrast, a large portion of the Re remained in an oxidized state even after reduction in H_2 at 393 and 473 K. Furthermore, the distribution of Re oxidation states was influenced by reduction over this narrow temperature range. After a 1 h reduction at 393 K, Re^0, Re^{2+}, and Re^{4+} were observed on both carbon-supported and silica-supported catalysts, and there was also a small percentage of Re^{7+} that was observed on the carbon-supported sample. The silica-supported catalyst appeared to be slightly more oxidized than the carbon-supported catalyst because the ratio of Re^{2+}/Re^0 in the silica-supported catalyst was higher. The same general behavior was observed after the catalysts were reduced at 473 K: the silica-supported catalyst appeared to be slightly more oxidized than the carbon-supported catalyst. As expected, the distribution of Re oxidation states was shifted toward Re metal when the catalysts were reduced at 473 K compared with 393 K, but there was still a significant amount of Re in the 2+ and 4+ oxidation states on both catalysts under all of the conditions studied.

The Re/Pt ratio of the catalysts as evaluated by XPS was also affected by the support and reduction temperature. In the rightmost column of Table 4, the areas under the photoemission response curves from Pt and Re were used to calculate the atomic ratio of Re/Pt associated with the bimetallic nanoparticles. The Re/Pt ratio for the carbon-supported catalyst did not appear to change as the catalyst was reduced at higher temperatures and the surface appeared to be slightly enriched in Re. The silica-supported catalyst, however, showed different behavior. As the reduction temperature was increased, the Re/Pt ratio indicates that the surface became enriched in Pt while Re segregated to the core of the catalytic particles.

2.3.2. Near Ambient Pressure X-ray Photoelectron Spectroscopy. Additional characterization of the Re in 8 wt % Pt−Re/C exposed to various environments was obtained using a synchrotron-based near-ambient-pressure X-ray photoelectron spectroscopy (NAP-XPS) system. The two major advantages of this system were (1) the ability to tune the photon energy of the X-ray source, which allowed a range of sample depths to be probed, and (2) the ability to perform measurements in the presence of reactant gases up to pressures of 0.3 mbar. Unfortunately, the silica-supported catalyst experienced significant charging effects during irradiation, and reliable spectra could not be acquired because this system was not amenable to utilizing charge compensation devices.

The NAP-XPS measurements were performed on 8 wt % Pt−Re/C at three different kinetic energies under several different environmental conditions. The kinetic energy was changed by tuning the incident photon energy for each element of interest so that the photon energy minus the binding energy of the element equaled the desired kinetic energy of the photoelectrons. By recording measurements at kinetic energies of 150, 500, and 1000 eV, the oxidation states of Pt and Re at different distances from the surface of the nanoparticles could be investigated. Table S5 shows the inelastic mean free path of the electrons from both Pt and Re at the three kinetic energies studied using the synchrotron-based technique as well as the inelastic mean free path of the conventional XPS experiments using Al Kα radiation. Because the photon energy could not be tuned in the conventional XPS experiments, the kinetic energy of photoelectrons differed for Pt and Re by 30 eV, which is the difference in binding energy for the two elements.

Figure 4 shows the NAP-XPS of 8 wt % Pt−Re/C at three different kinetic energies at 393 and 473 K in 0.3 mbar of H_2.

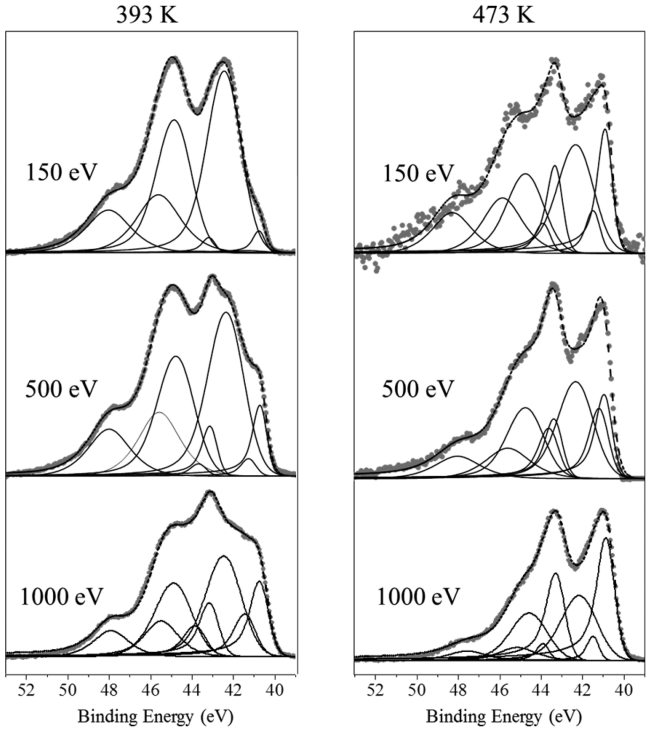

Figure 4. Re 4f NAP-XPS of 8 wt % Pt−Re/C, in 0.3 mbar of H_2 at 393 and 473 K, recorded at three different photoelectron kinetic energies. The gray dots are the data, and the dotted black lines are the results from peak fitting.

At both of these temperatures, the curve-fitting results show that as the kinetic energy of the photoelectrons increased, which corresponded to an increase in the probing depth, the oxidation state of the Re shifted toward Re metal. This result indicates that under reducing conditions at the temperatures studied, the Re closest to the surface of the nanoparticles was

DOI: 10.1021/acscatal.5b01371
ACS Catal. 2015, 5, 5679−5695

present in a range of oxidation states, and Re in the core of the nanoparticle had a lower oxidation state that was most likely metallic.

The NAP-XPS results of the Pt component of the catalyst, presented in Figure S4, revealed that the Pt was also in the metallic state. Since only one set of $4f_{7/2}$ and $4f_{5/2}$ peaks was observed in the spectra, we conclude that Pt resides primarily in a single state in the bimetallic samples. The binding energy of the Pt $4f_{7/2}$ peak was ~71.1 eV for the measurements obtained with kinetic energies of 500 and 1000 eV, which has been ascribed to metallic Pt.[61] The measurements obtained at a kinetic energy of 150 eV, however, revealed a shift in the binding energy of Pt of ~0.6 eV to around 71.7 eV. The Pt $4f_{7/2}$ binding energies for the NAP-XPS measurements are tabulated in Table S6. Duke et al. also observed a binding energy shift of ~0.55 eV in the Pt $4f_{7/2}$ peak upon the physical addition of Re to a Pt(111) single crystal using NAP-XPS at a photon energy of 545 eV.[57] Interestingly, when the Re was removed via oxidation at 500 K, the Pt $4f_{7/2}$ binding energy returned to that associated with the clean crystal at 71.0 eV. In addition, the Pt L_{III} XANES of alumina-supported[62] and Norit carbon-supported[4] Pt–Re nanoparticles were shifted to slightly higher energies than supported monometallic Pt nanoparticles. The fact that the white line intensity of the monometallic Pt was the same as that in the Pt–Re bimetallic sample indicates the Pt remained fully reduced in the presence of Re.[4] We ascribe the observed shift in the Pt $4f_{7/2}$ binding energy in the current work to an electronic interaction with Re on the surface of the nanoparticles. As mentioned above, the shift in binding energy was evident only at a kinetic energy of 150 eV, which suggests the affected Pt is mainly at the surface of the nanoparticles.

The quantitative results of the curve-fitting of the NAP-XPS experiments in 0.3 mbar of H_2 and the conventional XPS measurements after 8 wt % Pt–Re/C was treated in a separate reduction cell are shown in Table 5. Trends in the distribution of Re oxidation states in Table 5 show good agreement between the two different XPS techniques. Conventional XPS and NAP-XPS also show that the distribution of Re oxidation states shifts toward Re metal as the reduction temperature increased from 393 to 473 K, as indicated by the weighted average binding energy of the Re photoelectron response, which is tabulated in the table. Table 5 also presents conventional XPS and NAP-XPS results of the catalyst measured at room temperature in UHV. Again, these two techniques show general agreement in the distribution of Re oxidation states. Both techniques confirm that the Re on the surface of the catalyst was highly oxidized after it was exposed to air prior to any in situ reduction.

Because glycerol hydrogenolysis takes place in liquid water saturated with H_2, the influence of water on the distribution of Re oxidation states and the Re/Pt ratio was studied using NAP-XPS. The curve-fitting results of spectra taken at 150 eV, which are the most surface-sensitive measurements, are tabulated in Table 6, and the photoemission spectra are shown in Figure 5. Interestingly, when 0.15 mbar of H_2O was introduced with 0.15 mbar of H_2, little effect on the distribution of Re oxidation states, the binding energy of the Re species, and the Re/Pt ratio at 393 and 473 K was observed. Even when the H_2 was removed and 0.3 mbar H_2O was allowed to react with 8 wt % Pt–Re/C, no significant changes in the XPS response of the Re component of the catalyst were detected.

A separate experiment was then performed to test whether oxidation could be observed when a strong oxidant was introduced at a pressure of 0.3 mbar. The catalyst was first reduced at 393 K in situ, and an XPS measurement was recorded. The catalyst was then cooled to 333 K; 0.3 mbar of O_2 gas was introduced; and after 20 min, a NAP-XPS measurement was obtained. The results of this experiment are summarized in Figure 6 and Table 6. Severe oxidation of Re occurred at 333 K in the presence of O_2 compared with the reduced catalyst at 393 K. This control experiment indicates that oxidation of the Re did take place with an oxidant at the pressures used for the NAP-XPS technique.

Table 5. Composition and Distribution of Re Oxidation States in 8 wt % Pt–Re/C Catalyst Evaluated by Conventional and near-Ambient-Pressure XPS

	distribution of Re oxidation states					
kinetic energy, eV	Re(0), %	Re(II), %	Re(IV), %	Re(VII), %	av B.E. (eV)[a]	Re/Pt
			393 K[b]			
150	5	1	67	27	44.2	9.68
500	16	4	56	24	43.9	5.56
1000	28	16	42	14	43.3	4.29
1446[c]	39	13	45	3	42.6	1.78
			473 K[b]			
150	31	9	39	21	43.6	1.36
500	26	22	38	14	43.9	3.75
1000	53	6	33	7	42.7	3.58
1446[c]	59	11	31	0	42.1	2.21
			Room Temperature Before Reduction[d]			
150[e]	1	1	7	82	46.1	2.35
500	1	1	41	57	45.3	5.63
1000	0	2	51	47	44.9	4.73
1446[c]	7	0	11	81	45.6	1.80

[a]Weighted average binding energy. [b]Measurements performed in 0.3 mbar H_2 unless otherwise noted. [c]Measurements performed using conventional XPS with an Al Kα radiation source with a photon energy of 1486.8 eV. Thus, because Re has a binding energy of ~40 eV, the resulting photoelectrons have a kinetic energy of ~1446 eV. XPS measurements were also performed in UHV after reduction at the specified condition. [d]Measurements taken in UHV. [e]The curve-fitting of this measurement also showed 9% of the Re was in the (VI) oxidation state.

Table 6. Distribution of Re Oxidation States and the Re/Pt Atomic Ratio from NAP-XPS of 8 wt % Pt–Re/C at 393 and 473 K, a Kinetic Energy of 150 eV, and 0.3 mbar of Pressure

	Distribution of Re Oxidation States				
condition	Re(0), %	Re(II), %	Re(IV), %	Re(VII), %	Re/Pt
		393 K			
H_2	5	1	67	27	9.68
H_2 and H_2O	9	4	71	16	3.50
H_2O	6	4	75	15	3.51
O_2[a]	15	1	35	48	6.68
		473 K			
H_2	31	9	39	21	1.36
H_2 and H_2O	22	34	29	15	1.62
H_2O	27	23	34	15	1.39

[a]After reducing in H_2 at 393 K, the measurement was performed in O_2 at 333 K.

2.4. IR Spectroscopy of Adsorbed Pyridine. To characterize any Brønsted acid sites associated with the Pt–Re bimetallic nanoparticles, DRIFTS of adsorbed pyridine was

DOI: 10.1021/acscatal.5b01371
ACS Catal. 2015, 5, 5679–5695

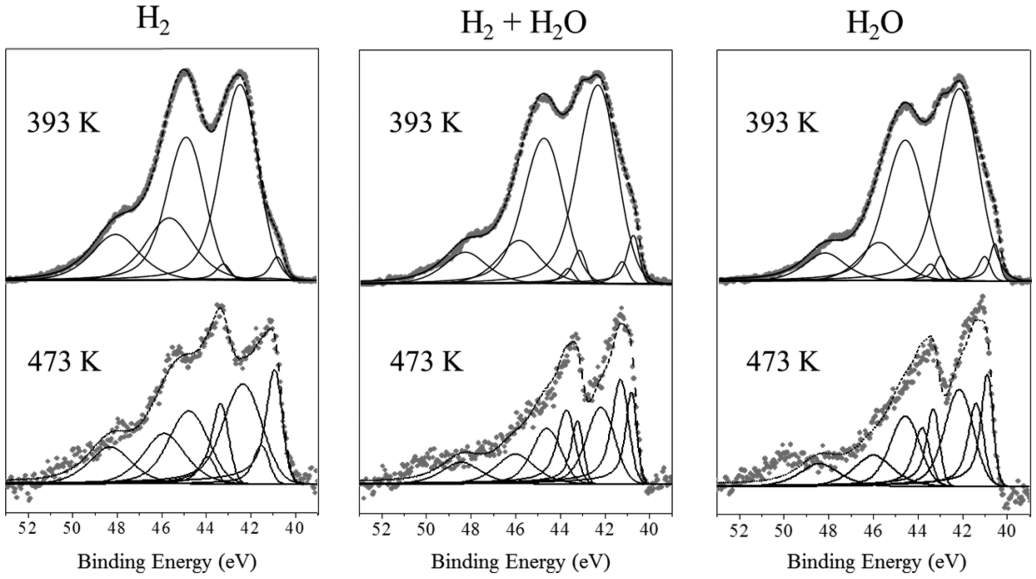

Figure 5. Re 4f NAP-XPS of 8 wt % Pt−Re/C at 393 and 473 K, a kinetic energy of 150 eV, and with 0.3 mbar of pressure of either H_2, H_2, and H_2O, or H_2O. The gray dots are the data, and the dotted black lines are the results from peak fitting.

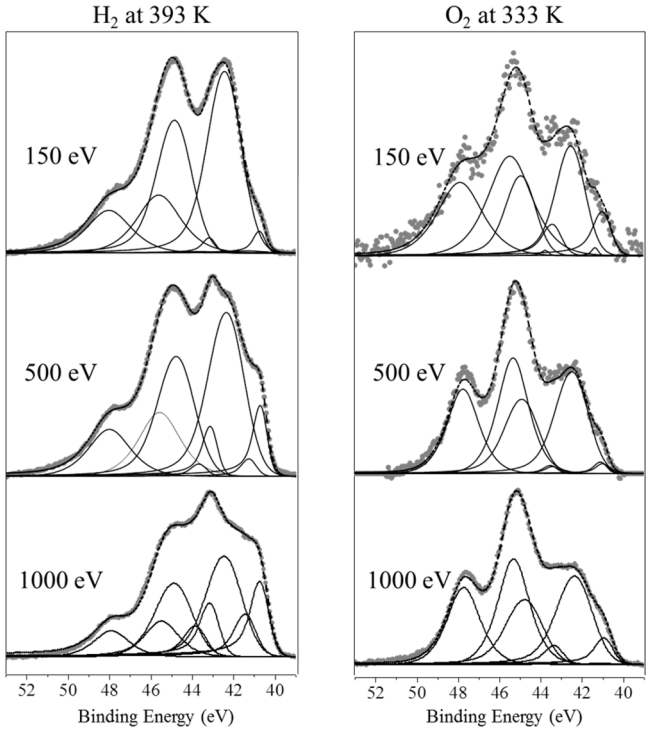

Figure 6. Comparison of Re 4f NAP-XPS of 8 wt % Pt−Re/C at 393 in 0.3 mbar of H_2 and at 333 K in O_2. The gray dots are the data, and the dotted black lines are the results from peak fitting.

used. Pyridine is a strong base that is commonly used to characterize acid sites on solid surfaces using IR spectroscopy because the IR signature of adsorbed pyridine is different when it is associated with a hydrogen bond, a Brønsted acid site, or a Lewis acid site.[44,63−69] Table S7 shows the IR absorption frequencies of the three vibrational modes (8a, 19a, and 19b) that are typically used to study the interaction of pyridine with solid surfaces. In this work, the silica-supported catalysts were used in the DRIFTS experiments because carbon-supported catalysts absorbed the IR radiation.

Spectra of pyridine adsorbed on 8 wt % Pt−Re/SiO_2−W and 8 wt % Pt/SiO_2, collected at 373 K after in situ reduction in H_2 at 473 K, are presented in Figure 7. The major peaks at 1597

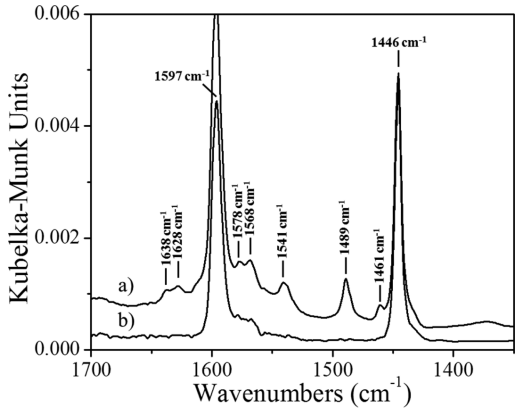

Figure 7. DRIFTS of adsorbed pyridine at 373 K after purging with He for 20 min on (a) 8 wt % Pt−Re/SiO_2−W and (b) 8 wt % Pt/SiO_2. Spectra are offset for clarity.

and 1446 cm^{-1} are associated with physically adsorbed pyridine, presumably on the silica support.[63−69] The peak located at 1541 cm^{-1} in Figure 7a is associated with the protonated pyridinium ion and therefore confirms the presence of Brønsted acid sites on 8 wt % Pt−Re/SiO_2−W. A spectrum of the unwashed catalyst showed the same features that can also be ascribed to pyridine bound to a Brønsted acid site. Figure 7b confirmed that acid sites were not present on 8 wt % Pt/SiO_2.

Zhang et al. and Ciftci et al. also observed Brønsted acid sites on silica-supported Pt−Re bimetallic catalysts revealed by IR spectroscopy of adsorbed pyridine.[12,34] In those works, however, the authors reported that the number of Brønsted acid sites increased when the catalysts were exposed to water vapor prior to pyridine. To investigate the role of water vapor, a DRIFTS experiment was conducted with 8 wt % Re/SiO_2 whereby water vapor was introduced at 473 K before the introduction of pyridine. Figure 8 compares the resulting

DOI: 10.1021/acscatal.5b01371
ACS Catal. 2015, 5, 5679−5695

spectrum from this experiment with a spectrum of 8 wt % Re/SiO_2 that was not pretreated with water.

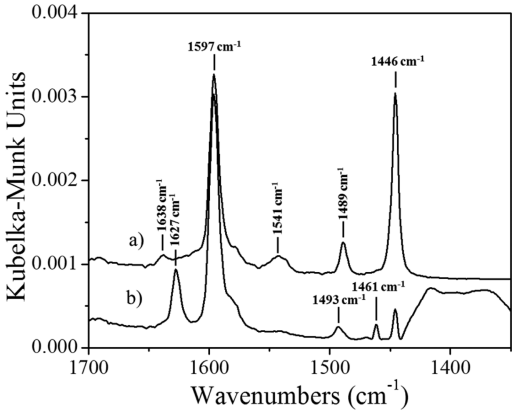

Figure 8. DRIFTS of adsorbed pyridine on 8 wt % Re/SiO_2 at 373 K after purging with He for 20 min (a) with the addition of water vapor and (b) without the addition of water vapor. Spectra are offset for clarity.

The spectra in Figure 8 suggest that, after reduction in H_2 at 473 K, Re supported on silica functions mainly as a Lewis acid for pyridine. The result is corroborated by the work of Kawai et al., who observed that higher reduction temperatures of Re/Al_2O_3 lowered the ratio of Brønsted acid sites to Lewis acid sites while maintaining the total amount of adsorbed pyridine.[70] The spectra in Figure 8 also suggest that the addition of water vapor hydrates the supported Re species and converts the Lewis acid sites to Brønsted acid sites. It is possible that catalysts pretreated with water vapor in the works by Zhang et al. and Ciftci et al. converted weakly held perrhenate species on the silica to Brønsted acid sites rather than converting bimetallic Pt−Re sites, which is why we probed a washed catalyst with soluble Re species removed from the surface. Nevertheless, DRIFTS of adsorbed pyridine confirms that Brønsted acid sites are associated with Pt−Re bimetallic particles, and the addition of water is not required to form active sites on catalysts reduced at 473 K.

2.5. Propyl Acetate Hydrolysis. The hydrolysis of propyl acetate, a well-known Brønsted acid-catalyzed reaction, was used to obtain an estimate of the number of acid sites present on the Pt−Re bimetallic catalysts in liquid water. The hydrolysis of aqueous esters has been commonly used as a probe reaction to characterize other solid acids.[71−73]

The conversion of propyl acetate was below the detectable limit at 333 K in 2.1 MPa of N_2 after 24 h of reaction in the absence of catalyst. The silica support and the Pt/SiO_2 catalyst did show a low hydrolysis activity, most likely from the few weak acid sites on SiO_2. For example, the conversion of propyl acetate after 24 h of reaction of the silica support was 0.2%, whereas the conversion on 8 wt % Pt/SiO_2 was slightly lower. The conversion of propyl acetate on 8 wt % Pt−Re/SiO_2 was 4.3% after 24 h, which was significantly higher than the silica support. The rate of propyl acetate hydrolysis remained constant on the bimetallic Pt−Re catalyst over the course of 28 h. Table 7 shows the conversions and rates of propyl acetate hydrolysis on 8 wt % Pt−Re/SiO_2 and 8 wt % Pt−Re/SiO_2−W measured after 8 h of reaction. A plot of the conversion as a function of time is shown in the Supporting Information (Figure S5). The 8 wt % Pt−Re/SiO_2−W catalyst exhibited

Table 7. Production of 1-Propanol from Propyl Acetate Hydrolysis[a]

catalyst	conversion[b] (%)	rate (μmol g^{-1} min^{-1})	H^+ equiv per Re
8 wt % Pt−Re/SiO_2	1.1	1.0	0.10
8 wt % Pt−Re/SiO_2−W	0.7	0.6	0.06
HCl (TOF[c] = 0.00039 s^{-1})	11.1		1

[a]Reaction conditions: 333 K, 2.1 MPa N_2, 8 h of reaction, substrate/Re(H^+) = 100, 150 cm^3 1.5 wt % propyl acetate solution. In situ pretreatment: 393 K, 1.4 MPa H_2, 1 h. [b]Based on 1-propanol production. [c]Based on total moles of H^+.

~60% of the rate of the 8 wt % Pt−Re/SiO_2 catalyst. Interestingly, the same fractional decrease in the rate of glycerol hydrogenolysis was also observed on the washed catalyst compared with the unwashed catalyst (Table 2). Evidently, the washing procedure removed ~30−40% of the Re sites that are active for both propyl acetate hydrolysis and glycerol hydrogenolysis. The higher propyl acetate hydrolysis rate of the Re-promoted Pt catalyst compared with Pt/SiO_2 supports the hypothesis that Pt−Re bimetallic particles contain acid sites after reduction in H_2 at 393 K, which participate in hydrolysis of propyl acetate at 333 K.

Propyl acetate hydrolysis was also performed with 8 wt % Pt/C and 8 wt % Pt−Re/C (not shown), but the bare Vulcan support had a very high activity, presumably as a result of surface carboxylic acid groups. Nevertheless, 8 wt % Pt−Re/C still had a higher rate than both the bare Vulcan support and the 8 wt % Pt/C catalyst.

To obtain an estimation of the number of Re atoms in the bimetallic catalyst that form acid sites, the rate of hydrolysis on the Pt−Re catalysts was compared with the rate of hydrolysis in aqueous HCl. Thus, a reaction was performed in which the amount of HCl used as a catalyst was equal to the nominal loading of Re used in a typical hydrolysis experiment with Pt−Re bimetallic catalyst. In Table 7, the ratio of the propyl acetate conversion on the Pt−Re catalysts to the conversion in aqueous HCl was then used to infer the number of H^+ equivalents on the Pt−Re catalyst. This measure suggests that ~10% of the Re on the unwashed catalyst forms Brønsted acid sites that are active for propyl acetate hydrolysis. Because the acid sites that catalyze hydrolysis on the unwashed catalyst can be attributed to the Pt−Re nanoparticles as well as adsorbed perrhenate, it may be more appropriate to conclude that the H^+ equivalents measured using 8 wt % Pt−Re/SiO_2−W was a better estimate of acid sites associated with the bimetallic clusters. Our results suggest that at least 6% of the Re on the catalyst forms Brønsted acid sites.

2.6. Selective Poisoning of Pt−Re Catalyst. To determine whether the Brønsted acid sites associated with the Re component of the Pt−Re bimetallic catalyst played a role in glycerol hydrogenolysis, the rate of the hydrogenolysis reaction was measured on a 4 wt % Pt−Re/C catalyst in the presence of NaOH. The physical characteristics of this particular catalyst are summarized in Table 1. A carbon-supported bimetallic catalyst was chosen for this set of experiments because silica is known to dissolve in aqueous solutions at high pH.[74] The results from glycerol hydrogenolysis in the presence of different concentrations of NaOH after 2 h of reaction are shown in Table 8.

Very small amounts of NaOH decreased the rate of glycerol hydrogenolysis significantly over 4 wt % Pt−Re/C. When a

DOI: 10.1021/acscatal.5b01371
ACS Catal. 2015, 5, 5679−5695

Table 8. Influence of NaOH and NaCl on Glycerol Hydrogenolysis over 4 wt % Pt−Re/C[a]

additive	Na/Re molar ratio	conversion (%)	rate (μmol g^{-1}min^{-1})	selectivites (%)				Sec/Prim
				1,2-PDO	1,3-PDO	2-Prop	1-Prop	
none		8.0	6.8	25	24	13	38	0.69
1 mM NaOH	0.5	6.5	5.3	28	25	18	30	0.59
10 mM NaOH	5	3.1	2.5	81	19	0	0	0.23
100 mM NaOH	50	3.2	2.9	78	5	0	0	0.07[b]
10 mM NaCl	5	7.8	6.7	23	27	14	36	0.73
100 mM NaCl	50	4.0	3.5	25	32	12	32	0.80

[a]Reaction conditions: 4 wt % Pt−Re/C, 393 K, 4 MPa H_2, 2 h of reaction, 90 cm^3 110 mM glycerol solution, Gly/Re = 50. In situ pretreatment: 393 K, 1.4 MPa H_2 for 1 h. [b]17% product selectivity to lactic acid was observed.

molar ratio of NaOH/Re = 0.5 was used, the rate of reaction decreased by 37%. The rate decreased even further when the NaOH/Re molar ratio increased to 5. At 100 mM NaOH, the rate actually increased while the selectivity to 1,3-PDO as well as the Sec/Prim ratio were very low. This increase in rate was attributed to a change in reaction mechanism because of the added base. Other studies have demonstrated base-catalyzed hydrogenolysis of the terminal C−O bonds of glycerol takes place in the presence of Pt at high pH.[4,26,27] In 100 mM NaOH, 17% of the product was actually lactate after 2 h of reaction, which also supports the change in reaction path. Clearly, addition of NaOH neutralized the acid sites responsible for activation of glycerol at the secondary carbon and increased the rate of terminal C−O bond activation, thus lowering the Sec/Prim ratio. Nevertheless, a significant decrease in the rate of glycerol hydrogenolysis was observed as the molar ratio of NaOH to Re was increased from 0 to 50 before a significant change in the reaction mechanism was reflected in the rate of reaction or the Sec/Prim ratio.

Additional experiments were performed in which NaCl was added to the reaction mixture in an attempt to decouple the possible influence of Na^+ on activity and selectivity. As shown in Table 8, the reaction with 10 mM NaCl revealed a rate and product selectivity that was approximately the same as the reaction without NaCl, indicating that the catalyst was not negatively affected by the addition of NaCl salt at these conditions. This result also suggests that the 63% decrease in rate observed in the presence of 10 mM NaOH can be attributed to the added presence of OH^-. Interestingly, the rate of glycerol hydrogenolysis decreased from 6.7 to 3.5 μmol g^{-1} min^{-1} when 100 mM NaCl was added to the reaction medium. It is possible that some of the sodium ions at high concentration exchanged with the acidic protons associated with the Brønsted acid sites created by the Pt−Re bimetallic nanoparticles or that the higher concentration of Cl^- may have negatively affected the Pt component of the catalyst, since it is well-known that the presence of Cl^- can coordinate to platinum group metals and negatively affect the catalytic activity.[26,75,76] Regardless of the effect on absolute activity, the Sec/Prim ratio remained very high in the presence of NaCl.

In summary, results from the addition of NaOH and NaCl to the reaction medium are consistent with the hypothesis that a Brønsted acid site associated with the Re component of the catalyst is critical in the activation of secondary C−O bonds during glycerol hydrogenolysis on Pt−Re bimetallic catalysts.

3. DISCUSSION

3.1. Oxidation State of Re. The extensive characterization of Pt−Re bimetallic nanoparticles revealed that Re existed in a variety of oxidation states when the Pt−Re samples were reduced in H_2 at 473 K or lower. Daniel et al. used X-ray absorption spectroscopy to study a Pt−Re bimetallic catalyst supported on Norit carbon and reported that the Re L_{III} edge energy shift of the catalyst reduced in H_2 at 473 K corresponded to an average Re oxidation state of ∼2+, which is in general agreement with our XPS results.[4] The Re L_{III} edge energy shift was also utilized by Koso et al. and Nakagawa et al. to characterize Rh−Re and Ir−Re bimetallic catalysts supported on silica, respectively, and they also reported that the average Re oxidation state was approximately 2+ after reduction in H_2 at 393 K.[40,55]

The Re/Pt atomic ratio, derived from XPS, of the silica-supported catalyst Pt−Re bimetallic catalyst decreased as the catalyst was reduced, indicating that Re segregated from the surface of the catalyst to the core of the catalyst under reducing conditions. Somorjai and coauthors have recently studied the restructuring of the PtPd and RhPd bimetallic systems under different reaction conditions using atomic ratios derived from a near-ambient-pressure synchrotron-based XPS technique similar to that used in this work.[77,78] The phenomena of Re segregation to the core with reduction at elevated temperatures is consistent with the model proposed by Chia et al. for Rh−Re nanoparticles.[8] In that work, EXAFS results indicated that bimetallic particles with a Re-rich core were formed at high reduction temperatures. Concurrent results from the catalytic hydrogenolysis of 2-(hydroxymethyl)tetrahydropyran showed that the rate decreased with increasing reduction temperature (up to 723 K), indicating that the number of active sites, which most likely require Re, decreased at the surface. The authors used CO chemisorption to rule out metal sintering as a cause for the decreased rate. Rhenium segregation to the core of Pt−Re bimetallic alloys is also consistent with calculations performed by Greely and Mavrikakis, which suggest that as Re/Pt alloys are heated to higher temperatures, the most stable configuration consists of subsurface Re with a Pt overlayer.[79]

3.2. The Nature of the Brønsted Acid Site. Results from this work confirm that Brønsted acid sites are present on the Pt−Re bimetallic catalysts and are most likely associated with the oxophilic Re component, which is consistent with NH_3-TPD results, suggesting that acid sites are also present on carbon-supported Rh−Re bimetallic catalysts.[7,8] The DRIFTS spectra in Figure 7 indicate that very few Lewis acid sites were present under the conditions of the experiment, and nearly all of the acid sites on the silica-supported Pt−Re nanoparticles could be attributed to Brønsted acid sites. These Brønsted acid sites were catalytically active for propyl acetate hydrolysis in liquid water. Because a catalyst that was washed to remove soluble perrhenate species weakly held to the silica support was still active for propyl acetate hydrolysis, we suggest the acid site is attributed to a partially oxidized Re species (Re oxidation

DOI: 10.1021/acscatal.5b01371
ACS Catal. 2015, 5, 5679−5695

state <7+) associated with Pt. Consistent with the idea that the acid site remains associated with the solid catalyst in liquid water, Chia et al. reported that Rh−Re bimetallic catalysts were active for the acid-catalyzed of hydrolysis of fructose to hydroxymethylfurfural in a continuous flow reactor for 250 h.[8]

3.3. The Role of Solvent in Hydrogenolysis on Pt−Re Catalysts. The results from this work also shed light on the role of water in glycerol hydrogenolysis. Pyridine DRIFTS showed that the addition of water is not required for Brønsted acid sites to be present on Pt−Re bimetallic nanoparticles. In addition, the NAP-XPS revealed that the addition of 0.3 mbar of water vapor does not change the oxidation state or binding energy of Re in the reduced catalyst, indicating that water does not react with or electronically alter the Re component of the catalyst significantly after the catalyst is reduced in H_2 at temperatures of 473 K and below. Moreover, the rate of glycerol hydrogenolysis was unchanged when D_2O was used as the solvent instead of H_2O. The hydrogenolysis of 1,2-HDO in an alkane solvent also confirms that water is not required to perform the selective hydrogenolysis of polyols.

3.4. Bifunctional Mechanism of Glycerol Hydrogenolysis on Pt−Re Catalysts. The extensive characterization of Pt−Re catalysts confirms that both metallic sites (associated with Pt) and acid sites (associated with partially oxidized Re) are present on the surface of the catalyst. One question that persists is the extent at which the acid site plays a role in the hydrogenolysis mechanism. For example, Chia et al. propose that the Brønsted acid sites selectively catalyze activation at secondary C−O bonds over primary C−O bonds (compared with metal-catalyzed hydrogenolysis) because secondary carbenium or oxocarbenium ions are more stable.[7] Indeed, acid-catalyzed dehydration of the secondary carbon of glycerol may form an unsaturated reactive intermediate that would be subsequently hydrogenated on Pt metal sites.

A competing mechanism is the direct hydrogenolysis of glycerol adsorbed on Pt−Re. The direct hydrogenolysis mechanism, favored by the group of Tomishige et al., suggests the heterolytic cleavage of H_2 on Pt−Re sites is involved in the reaction.[5,6]

Our work on the hydrogenolysis of glycerol$(OH)_3$-d_5 revealed a primary kinetic isotope effect of 2.0 ± 0.1 in liquid water, indicating that the activation of C−H bonds in glycerol is kinetically significant, which is consistent with the acid-catalyzed path described above. We should also note that C−H bond activation is also a proposed step in the metal-catalyzed hydrogenolysis of glycerol over Pt,[80] Ru,[80] and Rh[81] catalysts. Therefore, the kinetic isotope effect observed with glycerol-$(OH)_3$-d_5 cannot unambiguously discriminate between acid-catalyzed versus metal-catalyzed C−H bond activation during glycerol hydrogenolysis. Nevertheless, the observed primary kinetic isotope effect with glycerol$(OH)_3$-d_5 does not support a hydrogenolysis mechanism involving heterolytic cleavage of H_2 followed by the direct addition of hydrogen to activate C−O bonds in glycerol.

Chia et al. used quantum chemical calculations to show that a low energy path for glycerol hydrogenolysis over Rh−Re bimetallic catalysts is initiated by the protonation of an alcohol group by the Brønsted acid site of the catalyst.[7] Simultaneous with the elimination of water is an intramolecular hydride shift from a C−H bond on the adjacent CH_2−OH group to form an oxocarbenium ion (RCH−C═O$^{(+)}$H), which was claimed to be the most stable intermediate. The presence of an alcohol group at the β-carbon position lowered the reaction barrier by 14 kJ mol^{-1} by providing a back-side stabilization of the transition state. Moreover, the presence of water, in conjunction with the alcohol at the β-carbon, further aided in stabilizing the oxocarbenium ion transition state.[7]

Interestingly, we observed that both the rate of hydrogenolysis and the Sec/Prim ratio was lower when *n*-heptane was used as the solvent instead of water for the hydrogenolysis of 1,2-HDO. The presence of water may help to stabilize the oxocarbenium ion in the transition state of the concerted mechanism, whereas *n*-heptane cannot provide the back-side stabilization. This might explain why the rate of 1-hexanol production increased by a factor of 3 when water was used as the solvent instead of *n*-heptane in the hydrogenolysis of 1,2-HDO.

The order of reaction in both glycerol and H_2 at different glycerol concentrations also provides insights into the glycerol hydrogenolysis mechanism. As mentioned in Section 2.2.3, the orders of reaction have been reported elsewhere in the literature on similar catalysts, but the results are inconsistent. The kinetic analysis summarized in Figure 1 suggests that various orders can be found, depending on the conditions used.

Reaction kinetics that were measured in low concentrations of glycerol (15−65 mM) show that the reaction is first-order in glycerol concentration and approximately zero-order in H_2 pressure. In this regime, the surface appears to be saturated with enough hydrogen that perhaps hydrogenation is not kinetically significant and the acid-catalyzed activation and dehydration of glycerol is rate-determining. The reported TOF of hydrogenation of various carbonyl compounds on Pt catalysts at temperatures as high as 393 K is significantly greater than the rate of glycerol hydrogenolysis observed in this work.[82] In addition, the observed inverse kinetic isotope effect ($rate_H/rate_D = 0.7$) when D_2 was used as the reactant gas with a 15 mM glycerol solution suggests that the hydrogenation step may be equilibrated.[83,84] An inverse kinetic isotope effect may arise when two reactions with normal isotope effects of different magnitudes oppose each other,[83] and Bender et al. have measured equilibrium isotope effects for H_2 adsorption and desorption (K_H/K_D) of ∼0.7 for a few transition metal complexes, which agrees with the isotope effect we measured over Pt−Re.[84] Furthermore, Meemken et al. measured a normal kinetic isotope effect ($rate_H/rate_D$ = 1.4) with D_2 gas when studying the hydrogenation of a ketone on an alumina-supported Pt catalyst, confirming D_2 should produce a normal kinetic isotope effect when hydrogenation is a kinetically significant step.[85]

At higher concentrations of glycerol, where glycerol approaches zero-order behavior, an approximately half-order dependence on the H_2 pressure was observed. In this case, hydrogenation of an adsorbed unsaturated intermediate formed by the acid-catalyzed dehydration of glycerol may be kinetically significant. In classical hydrogenation kinetics on late transition metals, half-order dependence in H_2 corresponds to equilibrated adsorption of H_2 on a surface catalyzing hydrogen addition reactions. For exclusively metal-catalyzed glycerol hydrogenolysis reactions, the kinetically significant C−H bond activation step may result in a negative influence of H_2 pressure on the rate.[80] Indeed, the initial rate of glycerol hydrogenolysis over Pt[80] and Rh[81] was lower in H_2 relative to that in He or N_2.

In summary, the results presented in this work are consistent with a mechanism in which glycerol hydrogenolysis proceeds via acid-catalyzed dehydration/hydride shift, followed by

DOI: 10.1021/acscatal.5b01371
ACS Catal. 2015, 5, 5679−5695

hydrogenation of the resulting unsaturated intermediate. Intimate contact of the Brønsted acid (associated with the Re component of the catalyst) with the hydrogenation function (Pt) is necessary for high activity and selectivity for the activation of secondary alcohols.

4. CONCLUSIONS

The structure of the Pt−Re bimetallic catalyst was related to the function of the catalyst in glycerol hydrogenolysis in liquid water. Characterization of the Pt−Re catalysts with XPS revealed that Pt was completely reduced to Pt metal, but a distribution of Re oxidation states was observed on the bimetallic nanoparticles, even after reduction in H_2 at 473 K. In addition, NAP-XPS showed that water did not significantly alter the Re spectrum acquired at 393 and 473 K. Pyridine DRIFTS on Pt−Re/SiO_2 confirmed that Brønsted acid sites were present on the bimetallic nanoparticles after reduction in H_2, and these sites were active for propyl acetate hydrolysis in liquid water. By normalizing the rate of propyl acetate hydrolysis on Pt−Re/SiO_2 to the rate in HCl, we concluded that ∼6% of the Re's associated with the Pt−Re nanoparticles form Brønsted acid sites. The importance of the Brønsted acid sites in glycerol hydrogenolysis was confirmed by the addition of only 10 mM of NaOH to the reaction medium, which decreased the rate of glycerol hydrogenolysis by 60%. The NaOH evidently neutralized the Brønsted acid sites associated with the Re component of the catalyst. A primary kinetic isotope effect was also observed when glycerol$(OH)_3$-d_5 was used as the substrate, indicating the kinetic significance of C−H bond breaking in the glycerol hydrogenolysis mechanism. The characterization and reactivity results confirm the bifunctional nature of Pt−Re bimetallic catalysts and support a hydrogenolysis reaction path that involves acid-catalyzed dehydration, followed by metal-catalyzed hydrogenation.

5. EXPERIMENTAL METHODS

5.1. Catalyst Preparation. All catalysts were prepared by incipient wetness impregnation of metal precursors, followed by a thermal treatment. The Pt−Re bimetallic catalysts were synthesized by successive impregnation of the Pt precursor, followed by the Re precursor. The platinum precursor used was $Pt(NH_3)_4(NO_3)_2$ (Sigma-Aldrich), or H_2PtCl_6 (Sigma-Aldrich) if otherwise stated, and the Re precursor used for all of the catalyst was NH_4ReO_4 (Sigma-Aldrich). For a typical catalyst preparation, the Pt precursor was dissolved in a predetermined amount of distilled, deionized water to cause the silica gel support (Fuji Silysia G6) or the activated carbon support (Vulcan 72-XC) to reach incipient wetness. After the Pt solution was slowly added and thoroughly mixed with the support, the catalyst was dried overnight at 393 K in air. Then the Re precursor was dissolved in water, and the second impregnation was performed in the same manner. The catalyst was then dried overnight.

Before any measurements or reactions were performed, the bimetallic and monometallic Pt catalysts were heated at a rate of 0.5 K min^{-1} to 723 K and reduced for 3 h in 100 cm^3 min^{-1} of flowing H_2 (GTS Welco, 99.999%). After the catalysts were cooled to room temperature, a passivation gas (GTS Welco, 1.03% O_2 balance N_2) was introduced to the catalyst for 30 min. After passivation, the catalysts were stored in air at room temperature in a closed vial. The monometallic Re catalyst was calcined in flowing air at 773 K.

A procedure was also developed to remove spectator perrhenate that may be weakly held on the silica support of 8 wt % Pt−Re/SiO_2. Briefly, 1.5 g of 8 wt % Pt−Re/SiO_2 was loaded into a downward flow stainless steel tube with a K-type thermocouple placed into the reactor bed. The reactor was purged with flowing N_2 at atmospheric pressure for 30 min, followed by flowing H_2 for 30 min. Next, the catalyst was reduced in flowing H_2 at 473 K for 1 h at 1 MPa of pressure, which was maintained by a back-pressure regulator. The catalyst was then cooled in H_2 to 393 K, and distilled, deionized water, which was purged of air and saturated with 1 MPa of H_2, was introduced to the catalyst bed at a liquid flow rate of 2 cm^3 min^{-1} using an HPLC pump. After flowing for 30 min so that the number of residence times of liquid water in the reactor was ∼30, the water was purged from the system with H_2 and fully dried at 403 K in flowing H_2. The catalyst was subsequently cooled to room temperature and removed from the reactor. The resulting washed catalyst is referred to as 8 wt % Pt−Re/SiO_2−W.

5.2. Catalyst Characterization. The total number of hydrogen adsorption sites was determined by H_2 chemisorption using a Micromeritics ASAP 2020 automated adsorption analyzer. Samples were first heated at 4 K min^{-1} and reduced at 473 K in flowing H_2 for 1.5 h. Next, the samples were evacuated for 2 h at 473 K and then another 2 h at 308 K. After the evacuation, analysis was performed at 308 K in the pressure range of 75−450 Torr. The total number of hydrogen adsorption sites was calculated by extrapolating the total amount of H_2 adsorbed in the saturated region to zero pressure to remove contributions from physisorbed hydrogen. Elemental analysis (using ICP−OES performed by Galbraith Laboratories, 2323 Sycamore Drive, Knoxville, TN 37921) was used to determine the Pt and Re weight loadings of the Pt−Re bimetallic catalysts. Transmission electron microscopy (TEM) images of the catalysts were acquired with an FEI Titan operated at 300 kV and equipped with a Gatan 794 multiscan camera (EFTEM) and an energy dispersive spectrometer for elemental X-ray analysis. Samples for microscopy were prepared by dipping TEM grids into a mixture of ∼50 mg of catalyst and 7 cm^3 of cyclohexane, which was sonicated for 15 min. To evaluate the particle size of the sample, the diameters of over 300 individual particles were measured for each sample.

5.3. Polyol Hydrogenolysis. Glycerol hydrogenolysis reactions were performed in a 300 cm^3 Parr autoclave equipped with a glass liner, PID-controlled heater, magnetically driven stir bar, and a dip tube for periodic sampling. The reaction solution was prepared by diluting glycerol (Acros Organics, ACS grade) with distilled, deionized water. D_2O (Sigma-Aldrich, 99.9%), glycerol$(OH)_3$-d_5 (Cambridge Isotopes Laboratories, 99%), and D_2 gas (Cambridge Isotopes Laboratories, 99.8%) were also used when specified. For the selective poisoning experiments, NaOH (Sigma-Aldrich) and NaCl (Acros Organics) were dissolved in the reactant solution with glycerol. For a typical reaction, catalyst was loaded into the autoclave, and the solution was loaded into a separate reactant vessel that was wrapped with heating tape. The appropriate amount of catalyst was loaded into the empty reactor to give a ratio of moles of glycerol to total moles of Re (Gly/Re) equal to 150. In the experiments that the glycerol concentration was varied, a catalyst mass of 160 mg was maintained. After the contents were sealed in their respective containers, H_2 was used to purge the reactor and the reactant solution vessel for 20 min at atmospheric pressure. To rereduce the catalyst after exposure

DOI: 10.1021/acscatal.5b01371
ACS Catal. 2015, 5, 5679−5695

to air, an in situ reduction was performed at 393 K and 1.4 MPa of H_2 for 1 h. The reactant vessel was then heated to the reaction temperature of 393 K. When the reactant vessel reached the desired temperature, the solution was charged into the reactor, and the reactor was pressurized to the desired pressure with H_2. An initial sample of the reaction medium was taken through the dip tube while keeping the reactor sealed. The desired pressure of H_2 was maintained throughout the reaction by constantly feeding H_2. Samples were taken periodically throughout the course of the reaction and were analyzed using an Alliance high performance liquid chromatograph (Waters e2695) equipped with a refractive index detector (Waters 2414) and an Aminex ion exclusion column (Bio-Rad, HPX-87H) operating at 318 K with a 0.5 M H_2SO_4 mobile phase. Calibration curves were obtained using known volumes of reactants and products.

The conversion was calculated as the total moles of products divided initial moles of glycerol, and the selectivity for a specific product was the moles of that product divided by the total moles of product. The only products observed for glycerol hydrogenolysis at 393 K with H_2 in the headspace were 1,2-PDO, 1,3-PDO, 1-propanol (1-Prop), and 2-propanol (2-Prop); lactic acid was also observed when high concentrations of NaOH were used. All glycerol hydrogenolysis reactions performed in this work had a carbon balance between 90 and 105%. For simplicity, the ratio of C−O cleavages at secondary carbons versus primary carbons was calculated as the Sec/Prim ratio to compare selectivities for reactions performed with different catalysts. This number was calculated using the concentrations of the final products as shown below.

$$\frac{\text{Sec}}{\text{Prim}} = \frac{[\text{1,3-PDO}] + [\text{1-Prop}]}{[\text{1,2-PDO}] + 2[\text{2-Prop}] + [\text{1-Prop}]}$$

The procedure for hydrogenolysis of 1,2-hexanediol (1,2-HDO) was very similar to that used for glycerol hydrogenolysis. Solutions containing 110 mM of 1,2-HDO (Acros Organics, 98%) in distilled, deionized water or *n*-heptane (Sigma-Aldrich, 99%) were used as the reaction medium. Samples were analyzed using a gas chromatograph (Hewlett-Packard 5890 Series II) equipped with a flame ionization detector and a 50-m-long HP-1 cross-linked methyl silicone gum capillary column. Calibration curves were obtained using known volumes of reactants and products. The Sec/Prim ratio for 1,2-HDO hydrogenolysis was calculated as the ratio of 1-hexanol to 2-hexanol at various points throughout the reaction profile.

5.4. Propyl Acetate Hydrolysis. The reactor setup and procedure for propyl acetate hydrolysis were similar to those described in the previous section. The reactant solution for the hydrolysis experiment was prepared by mixing propyl acetate (Sigma-Aldrich, 99%) and 1-butanol (Sigma-Aldrich, 99.8%) with distilled, deionized water to give 1.5 and 0.1 wt % in propyl acetate and 1-butanol, respectively. The 1-butanol was used as an internal standard. The monometallic Pt and bimetallic Pt−Re catalysts were reduced in situ at 393 K with 1.4 MPa H_2, as described in Section 5.3, but after reduction, the reactor was purged four times with N_2 and cooled to the reaction temperature of 333 K. The reactants were then charged to the reactor, which was subsequently pressurized to 2.1 MPa in N_2. Samples were taken throughout the course of the reaction through a dip tube; after each sample, the reactor was backfilled with N_2 to keep the pressure in the reactor at 2.1 MPa. Samples were analyzed using a gas chromatograph (Hewlett-Packard 5890 Series II) equipped with a flame ionization detector and a 50-m-long HP-1 cross-linked methyl silicone gum capillary column. The conversion was calculated as the moles of 1-propanol formed divided by the moles of propyl acetate initially loaded into the reactor. Response factors were obtained using known volumes of reactants and products.

The appropriate amount of catalyst was loaded into the reactor in each experiment to ensure the ratio of moles of propyl acetate to total nominal moles of Re (or in the case of HCl, moles of H^+) was 100. The HCl (Fisher, Certified ACS Plus) was used as received.

5.5. X-ray Photoelectron Spectroscopy. Both conventional X-ray photoelectron spectroscopy (XPS) and near-ambient-pressure X-ray photoelectron spectroscopy (NAP-XPS) experiments were performed. Conventional XPS using a focused monochromatic Al Kα X-ray radiation source (1486.6 eV) and a Thermo Scientific ESCALAB 250 spectrometer was carried out at the Nanomaterials Core Characterization Facility of the Virginia Commonwealth University. A hemispherical analyzer with a six-element multichannel detector was used. The incident X-ray beam was 45° off normal to the sample, and the X-ray photoelectron detector was normal to the sample. A large-area magnetic lens with a 500 μm spot size in constant analyzer energy mode was utilized with a pass energy of 20 eV for region scans. Charge compensation was employed during data collection with an internal electron flood gun (2 eV) and a low-energy external Ar ion flood gun. Thirty region scans were taken with a step size of 0.1 eV for Pt and Re spectra.

Conventional XPS samples were prepared by pressing the powder catalyst onto a strip of Pb foil (ESPI Metals, 99.99%) that was secured onto a copper metal plate using an ultrahigh vacuum carbon paste (Ted Pella, PELCO); the copper plate was then attached to a sample holder. No Pb features were observed in the XPS survey scans, ensuring that the powder was thick enough that interactions between the Pb and the catalyst did not interfere with the measurements. To reduce the catalyst prior to conventional XPS analysis, the sample holder was placed in a reduction cell attached to the preparation chamber. After flushing the reduction cell three times with H_2 and pressurizing it to 0.2 MPa, the cell was heated to the desired temperature in H_2 for 1 h. After reduction, the cell was allowed to cool to room temperature, and the sample was transferred from the reduction cell to the preparation chamber, which was at a pressure of $\sim 10^{-6}$ mbar. The sample was then transferred from the preparation chamber over the course of about 5 min. The analysis chamber was maintained at a pressure of 10^{-9} mbar and was constantly purged with the Ar ion flood gun. To infer the amount of oxidation that occurred in the preparation chamber during the 5 min transfer, an experiment was performed during which the sample remained in the preparation chamber for 90 min after reduction.

The NAP-XPS experiments were performed at the Innovative Station for In Situ Spectroscopy (ISISS) beamline at the Helmholz-Zentrum Berlin/BESSY II synchrotron facility using a Phoibos 150 hemispherical energy analyzer. The advantages of this instrument were that the photon energy can be tuned between 80 and 2000 eV, and measurements can be made in pressures up to 0.3 mbar. More work using this system as well as a complete description of the equipment can be found elsewhere.[39,86−88] The pressure in the analysis chamber was maintained by simultaneous operation of mass flow controllers, to control the flow of gases, and a feedback-

DOI: 10.1021/acscatal.5b01371
ACS Catal. 2015, 5, 5679−5695

regulated valve between the chamber and a turbo molecular pump, to regulate the rate of pumping. The spectrometer utilizes a hemispherical analyzer that was operated in ultrahigh vacuum. The pressure difference between the reaction cell and the analyzer was maintained using three differentially pumped stages. Each stage consisted of an electrostatic lens for gathering a wide-angle spread of photoelectrons and focusing the electrons onto the analyzer entrance slit. Because this arrangement was not amenable to utilizing charge compensation devices, measurements were only performed using the 8 wt % Pt−Re/C catalyst. The silica-supported catalyst charged significantly, and reliable measurements could not be made.

For each condition studied, measurements were recorded at three different kinetic energies (150, 500, and 1000 eV) by adjusting the photon energy so that the difference between the photon energy and the kinetic energy equaled the appropriate binding energy. Spectra of Pt and Re were measured by averaging 30 scans using a pass energy of 10 eV and a step size of 0.05 eV. The total Gaussian resolution for the combination of photon source and spectrometer was 0.2 and 0.5 eV for the measurements with kinetic energies of 150 and 1000 eV, respectively. The core level binding energies for the NAP-XPS results were calibrated by first measuring the kinetic energy difference between the C 1s first and second order peaks to find the true kinetic energy of the C 1s first order peak, which was ∼284.2 eV. Next, the same photon energy used to obtain the Pt and Re spectra was used to measure C 1s binding energy at every condition studied. The Pt and Re peaks were then calibrated to those C 1s spectra, which were assigned to 284.2 eV. The accuracy of the binding energy calibration was estimated to be ∼0.1 eV.

The 8 wt % Pt−Re/C sample for NAP-XPS was prepared by first pressing the catalyst into a pellet. The pellet was then secured between one solid metal plate and one plate with a 3 mm diameter hole. The catalyst was heated via an infrared laser that was focused at the back of the solid metal plate using a fiber-optic cable and infrared optical elements. The temperature was measured with a K-type thermoelement that was secured between the metal plates in close proximity to the catalyst. In a typical experiment, the sample was loaded into the analysis chamber at room temperature and pressure of about 10^{-7} mbar. Next, H_2 was introduced at 5 cm^3 min^{-1} while the pressure was maintained at 0.3 mbar. The temperature was then increased to the desired temperature at a ramp rate of 10 K min^{-1}. The sample remained at the desired temperature for at least 20 min before any measurements were performed. Scans were recorded during the course of the experiment to ensure the catalyst was not changing and that it reached a stable state. After the measurement in the presence of H_2, H_2O and H_2 were introduced together, each at 5 cm^3 min^{-1}, and the system was allowed to equilibrate for 20 min before additional measurements were taken. Finally, the H_2 flow was halted so that only H_2O was introduced to the chamber. The H_2O was cryogenically distilled with liquid nitrogen to remove any air or other impurities.

For the silica-supported catalysts, the binding energies of all species were referenced to the Si 2p feature at 103.7 eV. The conventional XP spectra for the carbon-supported catalyst were referenced to the C 1s feature at 284.2 eV. Spectra obtained from both conventional XPS and NAP-XAS were deconvoluted with a curve-fitting routine in CasaXPS while using several constraints. For platinum and rhenium, the 7/2−5/2 spin−orbit coupling was set to 3.35 and 2.43 eV, respectively, and the 5/2 peak area was assigned to be 75% of the 7/2 peak area for both elements. The binding energies, fwhm, and lineshapes of the observed 7/2 Pt and Re species are shown in Table S8. The lineshapes of the 7/2 peaks were the same as the 5/2 peaks. Tougaard backgrounds were used to fit the Pt peaks, and Shirley backgrounds were used to fit the Re peaks. To calculate the Re/Pt molar ratio, the area under the photoemission response curves from Pt and Re, minus the background, were by corrected by the atomic subshell photoionization cross sections[89] and the photon flux in NAP-XPS.

5.6. Diffuse Reflection Infrared Fourier Transform Spectroscopy (DRIFTS) of Adsorbed Pyridine. The IR spectrum of pyridine adsorbed on the catalysts was recorded on a Bio-Rad FTIR (FTS-60A) spectrometer equipped with a liquid-nitrogen-cooled MCT detector and an in situ reactor cell for DRIFTS measurements (Harrick). To obtain spectra, 100 scans were coadded at a resolution of 2 cm^{-1}. The silica-supported samples used in DRIFTS were diluted in KBr powder (Varian Inc.) to give a 5 wt % catalyst mixture.

The loaded DRIFTS cell was first purged with 28 cm^3 min^{-1} of H_2 for 10 min and then heated to 473 K at a ramp rate of 10 K min^{-1} and reduced at 473 K in flowing H_2 for 1 h. After the catalyst was reduced, the cell was then purged at 473 K with 20 cm^3 min^{-1} of He for 15 min. Spectral backgrounds were then recorded at 373 and 303 K as the catalyst was cooled in He. At 303 K, a stream of pyridine vapor diluted in He was exposed to the sample for 1 min. The saturator containing pyridine was maintained at a temperature of 273 K. After adsorption of pyridine, the cell was purged with He, and the temperature of the cell was increased to 373 K to remove the majority of physisorbed pyridine prior to recording spectra. In separate experiments, a He water mixture was introduced to a reduced catalyst sample via a water saturator maintained at room temperature. The cell was then purged with He for 15 min at 473 K before any backgrounds were recorded after water adsorption.

■ ASSOCIATED CONTENT

Supporting Information

The Supporting Information is available free of charge on the ACS Publications website at DOI: 10.1021/acscatal.5b01371.

Additional information about the XPS curve fitting routine, the observation of ethanol evolution during propyl acetate hydrolysis, Tables S1−S8, and Figures S1−S5 (PDF)

■ AUTHOR INFORMATION

Corresponding Author

*Phone: 1−434−924−6284. E-mail: rjd4f@virginia.edu.

Notes

The authors declare no competing financial interest.

■ ACKNOWLEDGMENTS

The authors would like to acknowledge Dmitry Pestov and Professor Eric Carpenter in the Nanomaterials Characterization Center at Virginia Commonwealth University as well as Richard White in the Nanoscale Materials Characterization Facility at the University of Virginia. In addition, the authors acknowledge the UVA partnership with the Max Planck Society through MAXNET Energy. This material was based primarily upon the work supported by the National Science Foundation under Award Nos. CBET-1157829 and OISE-0730277. Helpful

DOI: 10.1021/acscatal.5b01371
ACS Catal. 2015, 5, 5679−5695

discussions with Qiaohua Tan, David Hibbitts, Matthew Neurock, Mei Chia, and James Dumesic as well as graphic rendering from Eric Dybeck are also acknowledged.

REFERENCES

(1) Simonetti, D.; Kunkes, E.; Dumesic, J. *J. Catal.* **2007**, *247*, 298−306.
(2) Kunkes, E.; Simonetti, D.; Dumesic, J.; Pyrz, W.; Murillo, L.; Chen, J.; Buttrey, D. *J. Catal.* **2008**, *260*, 164−177.
(3) King, D. L.; Zhang, L.; Xia, G.; Karim, A. M.; Heldebrant, D. J.; Wang, X.; Peterson, T.; Wang, Y. *Appl. Catal., B* **2010**, *99*, 206−213.
(4) Daniel, O. M.; DeLaRiva, A.; Kunkes, E. L.; Datye, A. K.; Dumesic, J. A.; Davis, R. J. *ChemCatChem* **2010**, *2*, 1107−1114.
(5) Koso, S.; Nakagawa, Y.; Tomishige, K. *J. Catal.* **2011**, *280*, 221−229.
(6) Amada, Y.; Shinmi, Y.; Koso, S.; Kubota, T.; Nakagawa, Y.; Tomishige, K. *Appl. Catal., B* **2011**, *105*, 117−127.
(7) Chia, M.; Pagán-Torres, Y. J.; Hibbitts, D.; Tan, Q.; Pham, H. N.; Datye, A. K.; Neurock, M.; Davis, R. J.; Dumesic, J. A. *J. Am. Chem. Soc.* **2011**, *133*, 12675−12689.
(8) Chia, M.; O'Neill, B. J.; Alamillo, R.; Dietrich, P. J.; Ribeiro, F. H.; Miller, J. T.; Dumesic, J. A. *J. Catal.* **2013**, *308*, 226−236.
(9) Dietrich, P. J.; Akatay, M. C.; Sollberger, F. G.; Stach, E. A.; Miller, J. T.; Delgass, W. N.; Ribeiro, F. H. *ACS Catal.* **2014**, *4*, 480−491.
(10) Dietrich, P. J.; Wu, T.; Sumer, A.; Dumesic, J. A.; Jellinek, J.; Delgass, W. N.; Ribeiro, F. H.; Miller, J. T. *Top. Catal.* **2013**, *56*, 1814−1828.
(11) Dietrich, P. J.; Sollberger, F. G.; Akatay, M. C.; Stach, E. A.; Delgass, W. N.; Miller, J. T.; Ribeiro, F. H. *Appl. Catal., B* **2014**, *156−157*, 236−248.
(12) Ciftci, A.; Ligthart, D. A. J. M.; Sen, A. O.; van Hoof, A. J. F.; Friedrich, H.; Hensen, E. J. M. *J. Catal.* **2014**, *311*, 88−101.
(13) Ciftci, A.; Ligthart, D. A. J. M.; Hensen, E. J. M. *Green Chem.* **2014**, *16*, 853−863.
(14) Takeda, Y.; Nakagawa, Y.; Tomishige, K. *Catal. Sci. Technol.* **2012**, *2*, 2221−2223.
(15) Xiao, J.; Puddephatt, R. J. *Coord. Chem. Rev.* **1995**, *143*, 457−500.
(16) Xiao, J.; Hao, L.; Puddephatt, R. J.; Manojlovic-Muir, L.; Muir, K. W. *J. Am. Chem. Soc.* **1995**, *117*, 6316−6326.
(17) Ebashi, T.; Ishida, Y.; Nakagawa, Y.; Ito, S.; Kubota, T.; Tomishige, K. *J. Phys. Chem. C* **2010**, *114*, 6518−6526.
(18) Kirilin, A. V.; Tokarev, A. V.; Manyar, H.; Hardacre, C.; Salmi, T.; Mikkola, J.-P.; Murzin, D. Y. *Catal. Today* **2014**, *223*, 97−107.
(19) Kim, Y. T.; Dumesic, J. A.; Huber, G. W. *J. Catal.* **2013**, *304*, 72−85.
(20) Mascal, M.; Dutta, S.; Gandarias, I. *Angew. Chem., Int. Ed.* **2014**, *53*, 1854−1857.
(21) Rahimpour, M. R.; Jafari, M.; Iranshahi, D. *Appl. Energy* **2013**, *109*, 79−93.
(22) Cortright, R. D.; Davda, R. R.; Dumesic, J. A. *Nature* **2002**, *418*, 964−967.
(23) Huber, G. W.; Shabaker, J. W.; Evans, S. T.; Dumesic, J. A. *Appl. Catal., B* **2006**, *62*, 226−235.
(24) Lehnert, K.; Claus, P. *Catal. Commun.* **2008**, *9*, 2543−2546.
(25) Wen, G.; Xu, Y.; Ma, H.; Xu, Z.; Tian, Z. *Int. J. Hydrogen Energy* **2008**, *33*, 6657−6666.
(26) Maris, E.; Davis, R. J. *J. Catal.* **2007**, *249*, 328−337.
(27) Maris, E.; Ketchie, W.; Murayama, M.; Davis, R. J. *J. Catal.* **2007**, *251*, 281−294.
(28) Miyazawa, T.; Kusunoki, Y.; Kunimori, K.; Tomishige, K. *J. Catal.* **2006**, *240*, 213−221.
(29) Furikado, I.; Miyazawa, T.; Koso, S.; Shimao, A.; Kunimori, K.; Tomishige, K. *Green Chem.* **2007**, *9*, 582−588.
(30) Shinmi, Y.; Koso, S.; Kubota, T.; Nakagawa, Y.; Tomishige, K. *Appl. Catal., B* **2010**, *94*, 318−326.
(31) Tamura, M.; Amada, Y.; Liu, S.; Yuan, Z.; Nakagawa, Y.; Tomishige, K. *J. Mol. Catal. A: Chem.* **2014**, *388−389*, 177−187.
(32) Koso, S.; Furikado, I.; Shimao, A.; Miyazawa, T.; Kunimori, K.; Tomishige, K. *Chem. Commun.* **2009**, 2035−2037.
(33) Chen, K.; Koso, S.; Kubota, T.; Nakagawa, Y.; Tomishige, K. *ChemCatChem* **2010**, *2*, 547−555.
(34) Zhang, L.; Karim, A. M.; Engelhard, M. H.; Wei, Z.; King, D. L.; Wang, Y. *J. Catal.* **2012**, *287*, 37−43.
(35) Wei, Z.; Karim, A. M.; Li, Y.; King, D. L.; Wang, Y. *J. Catal.* **2015**, *322*, 49−59.
(36) Vicente, B. C.; Nelson, R. C.; Moses, A. W.; Chattopadhyay, S.; Scott, S. L. *J. Phys. Chem. C* **2011**, *115*, 9012−9024.
(37) Hibbitts, D.; Tan, Q.; Neurock, M. *J. Catal.* **2014**, *315*, 48−58.
(38) Tysoe, W. T.; Zaera, F.; Somorjai, G. A. *Surf. Sci.* **1988**, *200*, 1−14.
(39) Greiner, M. T.; Rocha, T. C. R.; Johnson, B.; Klyushin, A.; Knop-Gericke, A.; Schlögl, R. *Z. Phys. Chem.* **2014**, *228*, 521−541.
(40) Koso, S.; Watanabe, H.; Okumura, K.; Nakagawa, Y.; Tomishige, K. *J. Phys. Chem. C* **2012**, *116*, 3079−3090.
(41) Amada, Y.; Watanabe, H.; Tomishige, K.; et al. *J. Phys. Chem. C* **2012**, *116*, 23503−23514.
(42) Baranowska, K.; Okal, J.; Miniajluk, N. *Catal. Lett.* **2014**, *144*, 447−459.
(43) Zhu, S.; Zhu, Y.; Hao, S.; Chen, L.; Zhang, B.; Li, Y. *Catal. Lett.* **2012**, *142*, 267−274.
(44) Zhu, S.; Qiu, Y.; Zhu, Y.; Hao, S.; Zheng, H.; Li, Y. *Catal. Today* **2013**, *212*, 120−126.
(45) Zhu, S.; Gao, X.; Zhu, Y.; Zhu, Y.; Xiang, X.; Hu, C.; Li, Y. *Appl. Catal., B* **2013**, *140−141*, 60−67.
(46) Zhu, S.; Gao, X.; Zhu, Y.; Cui, J.; Zheng, H.; Li, Y. *Appl. Catal., B* **2014**, *159*, 391−399.
(47) Chen, K.; Mori, K.; Watanabe, H.; Nakagawa, Y.; Tomishige, K. *J. Catal.* **2012**, *294*, 171−183.
(48) Nakagawa, Y.; Tomishige, K. *Catal. Surv. Asia* **2011**, *15*, 111−116.
(49) Chiang, Y.; Kresge, A. J.; Tang, Y. S.; Wirz, J. *J. Am. Chem. Soc.* **1984**, *106*, 460−462.
(50) Bohne, C.; MacDonald, I. D.; Dunford, H. B. *J. Am. Chem. Soc.* **1986**, *108*, 7867−7868.
(51) Chiang, Y.; Kresge, A. J.; Schepp, N. P. *J. Am. Chem. Soc.* **1989**, *111*, 3977−3980.
(52) Arceo, E.; Ellman, J. A.; Bergman, R. G. *J. Am. Chem. Soc.* **2010**, *132*, 11408−11409.
(53) Gandarias, I.; Arias, P. L.; Requies, J.; El Doukkali, M.; Güemez, M. B. *J. Catal.* **2011**, *282*, 237−247.
(54) Martin, A.; Armbruster, U.; Gandarias, I.; Arias, P. L. *Eur. J. Lipid Sci. Technol.* **2013**, *115*, 9−27.
(55) Nakagawa, Y.; Mori, K.; Chen, K.; Amada, Y.; Tamura, M.; Tomishige, K. *Appl. Catal., A* **2013**, *468*, 418−425.
(56) Tanuma, S.; Powell, C. J.; Penn, D. R. *Surf. Interface Anal.* **1994**, *21*, 165−176.
(57) Duke, A. S.; Galhenage, R. P.; Tenney, S. A.; Sutter, P.; Chen, D. A. *J. Phys. Chem. C* **2015**, *119*, 381−391.
(58) Komiyama, M.; Ogino, Y.; Akai, Y.; Goto, M. *J. Chem. Soc., Faraday Trans. 2* **1983**, *79*, 1719−1728.
(59) Cimino, A.; de Angelis, B. A.; Gazzoli, D.; Valigi, M. *Z. Anorg. Allg. Chem.* **1980**, *471*, 208−226.
(60) Chan, A. S. Y.; Chen, W.; Wang, H.; Rowe, J. E.; Madey, T. E. *J. Phys. Chem. B* **2004**, *108*, 14643−14651.
(61) Moulder, J. F.; Stickle, W. F.; Sobol, P. E.; Bomben, K. D. *Handbook of X-ray Photoelectron Spectroscopy*; Physical Electronics: Eden Prairie, MN, 1995.
(62) Hilbrig, F.; Michel, C.; Haller, G. L. *J. Phys. Chem.* **1992**, *96*, 9893−9899.
(63) Corrsin, L.; Fax, B. J.; Lord, R. C. *J. Chem. Phys.* **1953**, *21*, 1170−1176.
(64) Zaki, M. I.; Hasan, M. A.; Al-Sagheer, F. A.; et al. *Colloids Surf., A* **2001**, *190*, 261−274.
(65) Busca, G. *Catal. Today* **1998**, *41*, 191−206.

DOI: 10.1021/acscatal.5b01371
ACS Catal. 2015, 5, 5679−5695

(66) Andanson, J.; Baiker, A. *Chem. Soc. Rev.* **2010**, *39*, 4571−4584.
(67) Connell, G.; Dumesic, J. A. *J. Catal.* **1987**, *105*, 285−298.
(68) Emeis, C. A. *J. Catal.* **1993**, *141*, 347−354.
(69) Yuan, Q.; Yin, A. X.; Luo, C.; Sun, L. D.; Zhang, Y. W.; Duan, W. T.; Liu, H. C.; Yan, C. H. *J. Am. Chem. Soc.* **2008**, *130*, 3465−3472.
(70) Kawai, T.; Jiang, K. M.; Ishikawa, T. *J. Catal.* **1996**, *159*, 288−295.
(71) Namba, S.; Hosonuma, N.; Yashima, T. *J. Catal.* **1987**, *72*, 16−20.
(72) Segawa, K.; Sugiyama, A.; Kurusu, Y. *Stud. Surf. Sci. Catal.* **1991**, *60*, 73−80.
(73) Kimura, M.; Nakato, T.; Okuhara, T. *Appl. Catal., A* **1997**, *165*, 227−240.
(74) Maris, E. P.; Ketchie, W. C.; Oleshko, V.; Davis, R. J. *J. Phys. Chem. B* **2006**, *110*, 7869−7876.
(75) Marécot, P.; Fakche, A.; Kellali, B.; Mabilon, G.; Prigent, M.; Barbier, J. *Appl. Catal., B* **1994**, *3*, 283−294.
(76) Oh, H. S.; Yang, J. H.; Costello, C. K.; Wang, Y. M.; Bare, S. R.; Kung, H. H.; Kung, M. C. *J. Catal.* **2002**, *210*, 375−386.
(77) Tao, F.; Grass, M. E.; Zhang, Y.; Butcher, D. R.; Renzas, J. R.; Liu, Z.; Chung, J. Y.; Mun, B. S.; Salmeron, M.; Somorjai, G. A. *Science* **2008**, *322*, 932−934.
(78) Tao, F.; Grass, M. E.; Zhang, Y.; Butcher, D. R.; Aksoy, F.; Aloni, S.; Altoe, V.; Alayoglu, S.; Renzas, J. R.; Tsung, C. K.; Zhu, Z.; Liu, Z.; Salmeron, M.; Somorjai, G. A. *J. Am. Chem. Soc.* **2010**, *132*, 8697−8703.
(79) Greeley, J.; Mavrikakis, M. *Nat. Mater.* **2004**, *3*, 810−815.
(80) Wang, S.; Yin, K.; Zhang, Y.; Liu, H. *ACS Catal.* **2013**, *3*, 2112−2121.
(81) Auneau, F.; Michel, C.; Delbecq, F.; Pinel, C.; Sautet, P. *Chem. - Eur. J.* **2011**, *17*, 14288−14299.
(82) Ide, M. S.; Hao, B.; Neurock, M.; Davis, R. J. *ACS Catal.* **2012**, *2*, 671−683.
(83) Jones, W. D. *Acc. Chem. Res.* **2003**, *36*, 140−146.
(84) Bender, B. R.; Kubas, G. J.; Jones, L. H.; Swanson, B. I.; Eckert, J.; Capps, K. B.; Hoff, C. D. *J. Am. Chem. Soc.* **1997**, *119*, 9179−9190.
(85) Meemken, F.; Baiker, A.; Dupré, J.; Hungerbühler, K. *ACS Catal.* **2014**, *4*, 344−354.
(86) Bluhm, H.; Hävecker, M.; Knop-Gericke, A.; Kiskinova, M.; Schlögl, R.; Salmeron, M. *MRS Bull.* **2007**, *32*, 1022−1030.
(87) Klyushin, A. Y.; Rocha, T. C. R.; Hävecker, M.; Knop-Gericke, A.; Schlögl, R. *Phys. Chem. Chem. Phys.* **2014**, *16*, 7881−7886.
(88) Knop-Gericke, A.; Kleimenov, E.; Hävecker, M.; Blume, R.; Teschner, D.; Zafeiratos, S.; Schlögl, R.; Bukhtiyarov, V. I.; Kaichev, V. V; Prosvirin, I. P.; Nizovskii, A. I.; Bluhm, H.; Barinov, A.; Dudin, P.; Kiskinova, M. *Adv. Catal.* **2009**, *52*, 213−272.
(89) Yeh, J. J.; Lindau, I. *At. Data Nucl. Data Tables* **1985**, *32*, 1.

DOI: 10.1021/acscatal.5b01371
ACS Catal. 2015, 5, 5679−5695